# The ZZ Ceti Instability Strip for the Most Massive White Dwarf Pulsators

Gracyn Jewett[1] , Mukremin Kilic[1] , Adam Moss[2] , Alejandro H. Córsico[3,4] , Matthew J. Green[1] , Murat Uzundag[5] ,
Pierre Bergeron[6] , Warren R. Brown[7] , Francisco C. De Gerónimo[3,4] , Alberto Rebassa-Mansergas[8,9] , Alex J. Brown[10] ,
Vikram S. Dhillon[11,12] , and Stuart Littlefair[11]
[1] Homer L. Dodge Department of Physics and Astronomy, University of Oklahoma, 440 W. Brooks Street, Norman, OK 73019, USA; gjewett@ou.edu
[2] Department of Astronomy, University of Florida, Bryant Space Science Center, Stadium Road, Gainesville, FL 32611, USA
[3] Grupo de Evolución Estelar y Pulsaciones. Facultad de Ciencias Astronómicas y Geofísicas, Universidad Nacional de La Plata, Paseo delBosque s/n, (1900) La
Plata, Argentina
[4] Instituto de Astrofísica de La Plata, IALP (CCT La Plata), CONICET-UNLP, Argentina
[5] Institute of Astronomy, KU Leuven, Celestijnenlaan 200D, 3001, Leuven, Belgium
[6] Département de Physique, Université de Montréal, C.P. 6128, Succ. Centre-Ville, Montréal, QC H3C 3J7, Canada
[7] Center for Astrophysics, Harvard & Smithsonian, 60 Garden Street, Cambridge, MA 02138, USA
[8] Departament de Física, Universitat Politècnica de Catalunya, c/Esteve Terrades 5, 08860 Castelldefels, Spain
[9] Institut d'Estudis Espacials de Catalunya, Esteve Terradas, 1, Edifici RDIT, Campus PMT-UPC, 08860 Castelldefels, Barcelona, Spain
[10] Hamburger Sternwarte, University of Hamburg, Gojenbergsweg 112, 21029 Hamburg, Germany
[11] Astrophysics Research Cluster, School of Mathematical and Physical Sciences, University of Sheffield, Sheffield, S3 7RH, UK
[12] Instituto de Astrofísica de Canarias, E-38205 La Laguna, Tenerife, Spain

## Abstract

We present time-series photometry of 31 massive DA white dwarfs with $M \gtrsim 0.9\,M_\odot$ within the ZZ Ceti instability strip from the Montreal White Dwarf Database 100 pc sample. The majority of the targets had no previous time-series photometry available, though several were classified as nonvariable or potential pulsators in the literature. Out of the 31 candidates, we confirm 16 as pulsating. Our observations at three observatories have led us to discover the most massive pulsating white dwarf currently known, J0959−1828 ($M = 1.32$ or $1.27\,M_\odot$ for a CO versus ONe core), which is slightly more massive than the previous record holder J0049−2525. We study the sample properties of massive ZZ Ceti white dwarfs and find several trends with their weighted mean periods. As predicted by theory, we see an increase in the weighted mean periods with decreasing effective temperature and a decrease in pulsation amplitudes at the red edge of the instability strip. Furthermore, the weighted mean periods decrease with increasing stellar mass. Our observations show that the ZZ Ceti instability strip may not be pure at high masses. This is likely because the nonvariable white dwarfs in the middle of the strip may be weakly magnetic, which could escape detection in the available low-resolution spectroscopy data, but may be sufficient to suppress pulsations. Extensive follow-up observations of the most massive white dwarfs in our sample have the potential to probe the interior structures and core compositions of these white dwarfs with significantly crystallized cores.

*Unified Astronomy Thesaurus concepts:* ZZ Ceti stars (1847); White dwarf stars (1799); Stellar pulsations (1625)

## 1. Introduction

The vast majority of stars will evolve into white dwarfs (G. Fontaine et al. 2001; L. G. Althaus et al. 2010), and the majority of white dwarfs appear as DA white dwarfs, which have hydrogen dominated atmospheres. DA white dwarfs experience a phase of pulsations when they reach ∼12,000 K. Pulsating DA white dwarfs (DAVs) are commonly referred to as ZZ Cetis, named after the prototype of this class (A. U. Landolt 1968).

ZZ Ceti white dwarfs are found in a narrow temperature range between ≈10,400 and 12,400 K with periods ranging from 100 to 1400 s (A. H. Córsico et al. 2019). Pinpointing the exact boundaries of the instability strip is no small task (A. S. Mukadam et al. 2004; A. Gianninas et al. 2005; B. G. Castanheira et al. 2010; V. Van Grootel et al. 2012). An improved set of empirical boundaries were found by O. Vincent et al. (2020), who took advantage of Gaia parallaxes to constrain masses and used the results from several photometric surveys to define the boundaries of the instability strip (see their Figure 4).

The mass distribution of the white dwarfs in the solar neighborhood peaks at 0.6 $M_\odot$ with a broad shoulder and tail toward higher masses (M. Kilic et al. 2020, 2025; M. W. O'Brien et al. 2024), hence massive ($M \gtrsim 0.9\,M_\odot$) and ultramassive ($M \gtrsim 1.05\,M_\odot$) pulsating white dwarfs are rare. BPM 37093 is an ultramassive ZZ Ceti white dwarf with a mass of $1.037 \pm 0.008\,M_\odot$ (M. W. O'Brien et al. 2024) that was the most massive pulsator known at the time of its discovery (A. Kanaan et al. 1992). It is predicted that 90% of its core is crystallized (T. S. Metcalfe et al. 2004). J. J. Hermes et al. (2013) targeted GD 518 based on 1D model atmosphere fits to its optical spectrum, which indicated a mass of $1.20 \pm 0.03\,M_\odot$ (A. Gianninas et al. 2011). They detected three significant modes of pulsations in this star with periods ranging from 425 to 595 s, making it the most massive pulsating white dwarf known at the time. A model fit including Gaia parallaxes and the photometric method (P. Bergeron et al. 2019) results in a revised mass estimate of $1.114 \pm 0.006\,M_\odot$ for GD 518 (M. Kilic et al. 2025). Additional discoveries of massive pulsating white dwarfs include SDSS J084021.26+522217.8 (B. Curd et al. 2017),

which has $M = 0.98 \pm 0.04\,M_\odot$ (O. Vincent et al. 2024), and the most massive white dwarf known until now WDJ004917.14−252556.81 with $M = 1.312 \pm 0.010\,M_\odot$ (M. Kilic et al. 2023a; O. Caliskan et al. 2025).

G. Jewett et al. (2024) presented a detailed model atmosphere analysis of all white dwarfs with $M > 0.9\,M_\odot$ and $T_{\rm eff} \geqslant 11{,}000\,{\rm K}$ in the Montreal White Dwarf Database (MWDD; P. Dufour et al. 2017) 100 pc sample and the Pan-STARRS footprint. Because the temperature range of this sample of white dwarfs overlaps with the ZZ Ceti instability strip, they were able to identify massive DA white dwarfs that fell within the empirical boundaries of the strip. They found eight previously known pulsating massive white dwarfs and 14 objects that were not observed to vary (NOV) in this sample. They identified 22 ZZ Ceti candidates with no time-series follow-up at the time, including four objects with $M > 1.2\,M_\odot$. They also found several NOVs from O. Vincent et al. (2020) that fall right in the middle of the ZZ Ceti strip and identified J0135+5722 as one of the most interesting in that sample with $M = 1.15\,M_\odot$. F. C. De Gerónimo et al. (2025) have since confirmed multiperiodic pulsations in J0135+5722.

In order to identify massive and ultramassive pulsating white dwarfs and study the ZZ Ceti instability strip at the high mass end, we obtained time-series observations of 31 of the candidates identified by G. Jewett et al. (2024). Here we present the light curves and Fourier transforms for all 31 systems and provide a list of the significant frequencies detected for each object. This study provides a detailed view of the ZZ Ceti instability strip for the MWDD 100 pc sample of massive white dwarfs in the Pan-STARRS footprint.

In Section 2, we discuss the sample of white dwarfs studied in this paper, details of our observations, and the analysis of our data. Section 3 discusses the most massive pulsating white dwarfs in our sample in detail and presents the light curves and Fourier transforms for each star. Following this is a discussion of the nonvariable white dwarfs in Section 4. In Section 5, we explore trends in our data and discuss the purity of the ZZ Ceti instability strip for massive white dwarfs. Finally, we make our concluding remarks in Section 6.

## 2. Observations and Analysis

### 2.1. Sample

Table 1 presents the observational and physical parameters of the 31 ZZ Ceti candidates from G. Jewett et al. (2024). The masses range from $0.90\,M_\odot$ to $1.32\,M_\odot$ assuming CO cores, including 22 candidates with $M > 1\,M_\odot$. All but two of these targets have parallaxes $\geqslant 10$ mas. The two targets with smaller parallaxes, J1552+0039 and J1819+1225, are part of the MWDD 100 pc sample since that selection included objects with parallaxes consistent with being within 100 pc within $1\sigma$ based on Gaia DR2 astrometry. Note that time-series photometry for one of the candidates in the G. Jewett et al. (2024) sample, J0135+5722 (Gaia DR3 412839403319209600), was recently presented by F. C. De Gerónimo et al. (2025), hence we exclude it from this table.

Figure 1 shows the Gaia color–magnitude diagram with the massive MWDD 100 pc sample in gray, pulsating white dwarfs in green, and NOV white dwarfs in red. The pulsating (green) white dwarf sample includes both newly discovered pulsators presented in this work as well as previously known pulsators in the massive MWDD 100 pc sample. The same is

true for the NOV (red) white dwarfs shown. This figure shows the approximate boundaries of the ZZ Ceti instability strip for massive white dwarfs in the Gaia color–magnitude diagram. The MWDD 100 pc sample includes magnetic white dwarfs that fall within or near the instability strip, those are the gray triangles that fall near the pulsators in this diagram. The massive pulsators in our sample are located between $G_{\rm BP} - G_{\rm RP} = -0.06$ to $+0.09$ and $M_G = 12$–$14$.

### 2.2. Observations

Our primary telescope for observations was the 3.5 m at the Apache Point Observatory (APO). We used the Astrophysical Research Consortium Telescope Imaging Camera (ARCTIC) with the BG40 filter and $3 \times 3$ binning giving us a plate scale of $0\overset{''}{.}34$ per pixel. We typically obtained 10 s exposures over 2 hr for most targets. With an overhead of 4.5 s for each exposure, this results in a cadence of 14.5 s. The length of observations, significant frequencies, and $4\langle A \rangle$ detection limits where $\langle A \rangle$ is the average amplitude in the Fourier transform for the pulsators and NOVs are presented in Tables 2 and 7 (see Appendix B), respectively.

For one of our targets, J0959−1828, we were able to obtain follow-up observations with ULTRACAM (V. S. Dhillon et al. 2007), an ultra fast CCD camera, on the 3.5 m ESO New Technology Telescope (NTT) on UT 2025 March 28. ULTRACAM uses a triple beam setup and three frame transfer CCD cameras, which allows simultaneous data in three different filters with negligible (24 ms) dead time between exposures. We used the super-SDSS $u_s$, $g_s$, and $r_s$ filters (A. J. Brown et al. 2022). ULTRACAM observations were taken over 4 hr.

We were able to observe six of our targets (J0039−0357, J0204+8713, J0408+2323, J0657+7341, J0959−1828, and J1106+1802) using HiPERCAM (V. S. Dhillon et al. 2021), a high speed quintuple-beam CCD camera, on the 10.4 m Gran Telescopio Canarias (GTC). We used the super-SDSS $u_s$, $g_s$, $r_s$, $i_s$, and $z_s$ filters. All of the observations taken were over 4 hr, with the exceptions of J0408+2323 and J0959−1828.

### 2.3. Analysis

We used the Period4 software (P. Lenz 2005) to generate a Fourier transform for each night of observation in order to determine the significant pulsation frequencies. We applied a nonlinear least squares fitting procedure, where we identify the most significant peak above the detection threshold, fit it, and subtract the corresponding sinusoidal signal from the data, and repeat the process until no additional peaks exceeding the $4\langle A \rangle$ detection threshold are found. This detection threshold is defined as 4 times the average amplitude of the Fourier transform, which serves as the minimum amplitude for a frequency to be considered significant (M. Breger et al. 1993; O. Caliskan et al. 2025; F. C. De Gerónimo et al. 2025). This allowed us to accurately determine the frequency and amplitude of each pulsation mode. For observations with multiple bands, we process all of the data individually and include the frequencies detected in each filter in Table 3. We discuss the pulsating white dwarf sample in the next section and then present white dwarfs not-observed-to-vary in the following section.

**Table 1**
Observational and Physical Parameters of the ZZ Ceti Candidates Observed.

| Object Name | Gaia DR3 ID | R.A. (deg) | Decl. (deg) | Parallax (mas) | $G$ (mag) | $G_{BP}$ (mag) | $G_{RP}$ (mag) | log ($g$) (cgs) | $T_{eff}$ (K) | Mass $M_\odot$ | Cooling Age (Gyr) |
|---|---|---|---|---|---|---|---|---|---|---|---|
| J0039−0357 | 2527618112309283456 | 9.78326 | −3.95607 | 11.30 ± 0.22 | 18.61 | 18.62 | 18.67 | 9.20 | 11871 ± 214 | 1.271 ± 0.009 | 2.09 ± 0.06 |
| J0050−2826 | 2342438501397962112 | 12.71700 | −28.43495 | 11.07 ± 0.11 | 17.81 | 17.86 | 17.80 | 8.73 | 11320 ± 155 | 1.061 ± 0.011 | 1.72 ± 0.08 |
| J0127−2436 | 5040290528701395456 | 21.89464 | −24.60557 | 12.36 ± 0.19 | 18.69 | 18.74 | 18.69 | 9.24 | 11236 ± 214 | 1.284 ± 0.009 | 2.22 ± 0.06 |
| J0154+4700 | 356186555597277440 | 28.64365 | 47.01313 | 10.21 ± 0.12 | 17.93 | 17.95 | 17.96 | 8.76 | 11838 ± 235 | 1.077 ± 0.014 | 1.59 ± 0.10 |
| J0158−2503 | 5121833510769131136 | 29.69913 | −25.05308 | 11.21 ± 0.10 | 17.79 | 17.79 | 17.80 | 8.84 | 12234 ± 94 | 1.122 ± 0.007 | 1.68 ± 0.04 |
| J0204+8713 | 575585919005741184 | 31.12914 | 87.22579 | 11.11 ± 0.08 | 17.79 | 17.85 | 17.78 | 8.71 | 11135 ± 207 | 1.053 ± 0.015 | 1.75 ± 0.11 |
| J0408+2323 | 53716846734195328 | 62.01259 | 23.39512 | 12.40 ± 0.09 | 17.29 | 17.32 | 17.30 | 8.66 | 12053 ± 110 | 1.024 ± 0.008 | 1.22 ± 0.06 |
| J0538+3212 | 3447991090873280000 | 84.74184 | 32.20788 | 10.30 ± 0.10 | 17.51 | 17.53 | 17.57 | 8.61 | 12454 ± 154 | 0.994 ± 0.010 | 0.95 ± 0.05 |
| J0634+3848 | 945007674022721280 | 98.56907 | 38.81528 | 21.88 ± 0.04 | 15.73 | 15.74 | 15.75 | 8.50 | 12210 ± 106 | 0.926 ± 0.006 | 0.81 ± 0.02 |
| J0657+7341 | 1114813977776610944 | 104.29631 | 73.69572 | 11.86 ± 0.09 | 17.65 | 17.67 | 17.68 | 8.86 | 12609 ± 119 | 1.134 ± 0.007 | 1.61 ± 0.05 |
| J0712−1815 | 2934281803636268416 | 108.08535 | −18.26537 | 17.87 ± 0.05 | 16.40 | 16.41 | 16.41 | 8.59 | 11742 ± 136 | 0.980 ± 0.008 | 1.09 ± 0.05 |
| J0725+0411 | 3139633462883694976 | 111.45264 | 4.19282 | 11.37 ± 0.08 | 17.22 | 17.23 | 17.26 | 8.53 | 12022 ± 88 | 0.940 ± 0.008 | 0.88 ± 0.02 |
| J0912−2642 | 5649808720867457664 | 138.11673 | −26.70103 | 27.48 ± 0.04 | 16.41 | 16.40 | 16.46 | 9.17 | 12973 ± 115 | 1.262 ± 0.002 | 1.84 ± 0.03 |
| J0949−0730 | 3819743428284589696 | 147.41109 | −7.501786 | 12.42 ± 0.08 | 17.32 | 17.33 | 17.39 | 8.77 | 12941 ± 184 | 1.084 ± 0.008 | 1.26 ± 0.07 |
| J0950−2841 | 5464929134894103808 | 147.74005 | −28.68750 | 12.76 ± 0.09 | 17.34 | 17.31 | 17.41 | 8.84 | 13335 ± 203 | 1.124 ± 0.006 | 1.35 ± 0.06 |
| J0959−1828 | 5671878015177884032 | 149.88858 | −18.47373 | 12.76 ± 0.09 | 18.13 | 18.15 | 18.14 | 9.38 | 11995 ± 176 | 1.320 ± 0.004 | 1.83 ± 0.05 |
| J1052+1610 | 3981634249048141440 | 163.15010 | 16.17275 | 13.39 ± 0.12 | 17.27 | 17.29 | 17.26 | 8.66 | 11256 ± 84 | 1.020 ± 0.009 | 1.52 ± 0.06 |
| J1106+1802 | 3983606596814071680 | 166.51878 | 18.04182 | 12.33 ± 0.09 | 17.51 | 17.51 | 17.55 | 8.86 | 12877 ± 269 | 1.131 ± 0.011 | 1.51 ± 0.09 |
| J1243+4805 | 1543370904111505408 | 190.92339 | 48.09304 | 12.51 ± 0.05 | 16.97 | 16.96 | 17.02 | 8.57 | 12751 ± 101 | 0.966 ± 0.006 | 0.81 ± 0.02 |
| J1342−1413 | 3606080968656361344 | 205.67123 | −14.22819 | 20.54 ± 0.04 | 15.98 | 16.00 | 15.96 | 8.47 | 11351 ± 66 | 0.902 ± 0.006 | 0.93 ± 0.02 |
| J1451−2502 | 6229330032504603136 | 222.96896 | −25.04411 | 12.63 ± 0.15 | 17.39 | 17.43 | 17.37 | 8.65 | 11189 ± 97 | 1.016 ± 0.011 | 1.53 ± 0.07 |
| J1552+0039 | 4410623858974488832 | 238.15940 | 0.65268 | 9.72 ± 0.25 | 18.49 | 18.48 | 18.55 | 9.12 | 13508 ± 233 | 1.245 ± 0.011 | 1.70 ± 0.05 |
| J1626+2533 | 1304081783374935680 | 246.74813 | 25.55767 | 11.88 ± 0.07 | 17.59 | 17.60 | 17.66 | 8.87 | 13202 ± 189 | 1.140 ± 0.007 | 1.46 ± 0.06 |
| J1656+5719 | 1433629812475800320 | 254.16291 | 57.31760 | 12.69 ± 0.07 | 17.40 | 17.43 | 17.41 | 8.70 | 11551 ± 143 | 1.047 ± 0.010 | 1.54 ± 0.07 |
| J1722+3958 | 1346883876962000000 | 260.66923 | 39.96965 | 10.30 ± 0.07 | 17.81 | 17.82 | 17.78 | 8.62 | 11069 ± 109 | 0.997 ± 0.010 | 1.45 ± 0.07 |
| J1819+1225 | 4484736543328721792 | 274.85822 | 12.43255 | 9.77 ± 0.13 | 18.13 | 18.13 | 18.11 | 8.83 | 11929 ± 185 | 1.116 ± 0.012 | 1.76 ± 0.08 |
| J1928+1526 | 4321498378443922816 | 292.06065 | 15.44412 | 10.26 ± 0.10 | 17.73 | 17.75 | 17.73 | 8.64 | 11621 ± 141 | 1.011 ± 0.012 | 1.31 ± 0.08 |
| J1929−2926 | 6764486080026955136 | 292.30264 | −29.44520 | 11.28 ± 0.16 | 17.69 | 17.71 | 17.71 | 8.72 | 11455 ± 220 | 1.054 ± 0.016 | 1.62 ± 0.12 |
| J2026−2254 | 6849850998873128704 | 306.69792 | −22.91429 | 14.20 ± 0.08 | 16.79 | 16.80 | 16.79 | 8.49 | 11405 ± 88 | 0.917 ± 0.008 | 0.95 ± 0.03 |
| J2107+7831 | 2284856630775525376 | 316.96357 | 78.53158 | 10.15 ± 0.08 | 17.83 | 17.82 | 17.92 | 8.79 | 12707 ± 202 | 1.099 ± 0.009 | 1.41 ± 0.08 |
| J2208+2059 | 1781605382738862592 | 332.13117 | 20.98618 | 11.09 ± 0.09 | 17.48 | 17.55 | 17.46 | 8.53 | 11091 ± 99 | 0.941 ± 0.011 | 1.12 ± 0.05 |

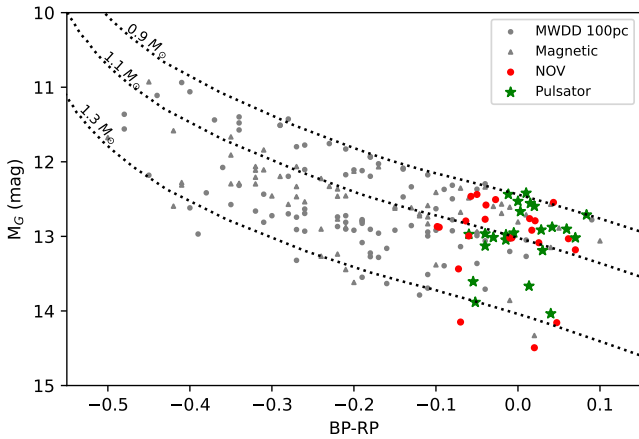**Note.** Mass and cooling age estimates are based on CO-core models (G. Jewett et al. 2024).

**Figure 1.** Color–magnitude diagram of the massive ($M > 0.9\,M_\odot$) white dwarfs with $T_{\text{eff}} \geqslant 11{,}000$ K in the MWDD 100 pc sample and the Pan-STARRS footprint from G. Jewett et al. (2024). The dotted lines show the evolutionary sequences for 0.9, 1.1, and 1.3 $M_\odot$ white dwarfs with C/O cores (top to bottom, P. Bergeron et al. 2019). The green stars mark both the previously known and the newly discovered pulsating white dwarfs in the sample. Similarly, the red points mark the previously known and newly discovered NOVs.

### 3. Pulsating White Dwarfs

With our photometric follow-up, we confirm pulsations in 14 new massive white dwarfs. G. Jewett et al.'s (2024) sample contains 10 previously known massive pulsating ZZ Ceti white dwarfs, including the most massive pulsator previously known J0049−2525 (M. Kilic et al. 2023a; O. Caliskan et al. 2025) and the recently presented J0135+5722 (F. C. De Gerónimo et al. 2025). The frequencies we deem significant (amplitudes above the $4\langle A \rangle$ detection threshold) are marked by dashed blue lines on the Fourier transforms presented below and are listed in Table 2 along with their amplitudes and periods. The masses and effective temperatures for each white dwarf are adopted from G. Jewett et al. (2024) and can be found in Table 1.

In this section, we present the light curves and corresponding Fourier transforms for six systems with $M > 1.1\,M_\odot$. The remaining systems are presented in Appendix A.

#### 3.1. J0039−0357

J0039−0357 has $M = 1.271 \pm 0.009\,M_\odot$ and $T_{\text{eff}} = 11{,}871 \pm 214$ K. It is one of the most interesting pulsators that we found as we see changing pulsation modes on four different nights of observations. The light curves and corresponding Fourier transforms are shown in Figure 2. On the first night of observation, UT 2024 October 9, we detect four modes with frequencies of 305.8, 318.0, 330.3, and 632.9 c day$^{-1}$. The mode at 632.9 c day$^{-1}$ is likely a combination frequency of the modes at 305.8 and 330.3 c day$^{-1}$ as the mode is the sum of these two frequencies. The highest amplitude we detect is for the mode at 318.0 c day$^{-1}$ at 32.3 millimodulation amplitude (mma). The next night of observations was on UT 2024 November 6, this drops down to just two modes detected with frequencies of 329.5 and 664.2 c day$^{-1}$, with the latter being a harmonic ($2\times$) of the former. The first mode has an amplitude of 33.6 mma.

The third night of observations on UT 2024 December 1 shows the richest pulsation spectrum for this object. We detect seven modes with frequencies ranging from 236.8 to 891.4 c day$^{-1}$. Several of these modes are likely combination

frequencies. For example, the mode at 562.3 c day$^{-1}$ is a combination of 236.8 and 327.8 c day$^{-1}$, and 891.4 c day$^{-1}$ is a combination of 327.8 and 562.3 c day$^{-1}$. The highest amplitude mode is at 318.3 c day$^{-1}$ with an amplitude of 13.0 mma. Then, on UT 2024 December 23, we find three modes with frequencies of 330.9, 663.8, and 674.6 c day$^{-1}$, with the last two likely being combination frequencies. The first mode at 330.9 c day$^{-1}$ has the highest amplitude of 23.9 mma. Finally, we also observed J0039−0357 at GTC shown in Figure 3. The $g$-band data shows modes at 319.2, 330.9, and 658.2 c day$^{-1}$. The dominant mode at 330.9 c day$^{-1}$ is detected in each filter, with decreasing amplitudes in the redder filters, and its harmonic at 658.2 c day$^{-1}$ is detected in the $u$- and $g$-bands. Clearly, we are seeing some modes disappear and some appear on different nights. The mode at $\approx 330$ c day$^{-1}$ is present on each night of observation, but with amplitudes ranging from 12 to 34 mma. This seems to be the only mode that we can consistently detect during each observation.

#### 3.2. J0158−2503

J0158−2503 has $M = 1.122 \pm 0.007\,M_\odot$ and $T_{\text{eff}} = 12{,}234 \pm 94$ K. We observed this white dwarf on two different nights, UT 2024 December 9 and 25. The light curves and corresponding Fourier transforms are shown in Figure 4. On the first night of observing, we find there to be two significant modes with frequencies of 185.5 and 205.9 c day$^{-1}$. The amplitudes of these modes are 5.4 and 30.1 mma, respectively.

Interestingly, on the second night of observations, we detect five modes with frequencies of 195.8, 205.3, 216.7, 411.5, and 422.2 c day$^{-1}$. The dominant mode at 205.3 c day$^{-1}$ has an amplitude of 46.2 mma. Two of the modes are likely combination frequencies: 411.5 c day$^{-1}$ is a combination of 195.8 and 205.3 c day$^{-1}$, and 422.2 c day$^{-1}$ is a combination of 205.3 and 216.7 c day$^{-1}$. We see the mode at $\approx 205$ c day$^{-1}$ on both nights of observations, but the amplitudes clearly change on each night.

#### 3.3. J0912−2642

J0912−2642 has $M = 1.262 \pm 0.002\,M_\odot$ and $T_{\text{eff}} = 12{,}973 \pm 115$ K. We were able to observe J0912−2642 on two nights. On UT 2024 November 23, we detected two modes at 85.3 and 91.7 c day$^{-1}$ with fairly low amplitudes of 2.3 mma and 1.8 mma, respectively. The second night, UT 2025 February 5, revealed no significant modes. Figure 5 shows the light curves and Fourier transforms. Given the two modes detected on the first night of observations, we tentatively classify this as a pulsator. However, additional time-series data are needed to confirm pulsations and study the pulsation spectrum of this ultramassive white dwarf.

#### 3.4. J0959−1828

This white dwarf was previously observed for five nights by M. Kilic et al. (2023b) at three different observatories. Their observations indicated that J0959−1828 is possibly pulsating, but their data was inconclusive as they detected significant modes above the $4\langle A \rangle$ limit only in one of the five nights of observations.

J0959−1828 is an exciting find in our follow-up sample, as it has a mass of $M = 1.320 \pm 0.004\,M_\odot$ assuming a CO core. Figure 6 shows its APO (top) and NTT/ULTRACAM (bottom panels) light curves and Fourier transforms. Our APO observations reveal a significant mode at $401.2 \pm 0.8$ c day$^{-1}$ with an amplitude of 7.4 mma. We confirm this pulsation mode

**Table 2**
Observation Details and Significant Frequencies for the Pulsators from APO and NTT

| Observation (UT Date) | Length (hr) | Frequency (cycles per day) | Amplitude (mma) | Period (s) | $4\langle A\rangle$ (mma) |
|---|---|---|---|---|---|
| J0039−0357 2024 Oct 9 | 2.1 | F1 305.806161 ± 0.852963 | 8.8 ± 1.2 | 282.531914 ± 0.788046 | 6.7 |
| | | F2 318.017123 ± 0.232395 | 32.3 ± 1.2 | 271.683484 ± 0.198536 | |
| | | F3 330.304311 ± 0.293023 | 25.6 ± 1.2 | 261.576967 ± 0.232053 | |
| | | F4 632.896625 ± 0.858287 | 8.8 ± 1.2 | 136.515185 ± 0.185132 | |
| J0039−0357 2024 Nov 6 | 1.8 | F1 329.545632 ± 0.228252 | 33.6 ± 1.0 | 262.179169 ± 0.181592 | 4.9 |
| | | F2 664.211752 ± 1.113189 | 6.9 ± 1.0 | 130.078999 ± 0.218007 | |
| J0039−0357 2024 Dec 1 | 4.0 | F1 236.758272 ± 0.311809 | 7.5 ± 0.7 | 364.929171 ± 0.480609 | 3.7 |
| | | F2 303.799586 ± 0.186465 | 12.6 ± 0.7 | 284.398018 ± 0.174557 | |
| | | F3 318.330153 ± 0.180977 | 13.0 ± 0.7 | 271.416324 ± 0.154306 | |
| | | F4 327.816169 ± 0.190752 | 12.3 ± 0.7 | 263.562350 ± 0.153364 | |
| | | F5 373.159609 ± 0.516541 | 4.5 ± 0.7 | 231.536313 ± 0.320501 | |
| | | F6 562.340182 ± 0.203228 | 11.5 ± 0.7 | 153.643653 ± 0.055526 | |
| | | F7 891.439809 ± 0.398957 | 5.9 ± 0.7 | 96.921855 ± 0.043377 | |
| J0039−0357 2024 Dec 23 | 3.9 | F1 330.929490 ± 0.112032 | 23.9 ± 0.8 | 261.082806 ± 0.088386 | 4.0 |
| | | F2 663.787672 ± 0.437500 | 6.1 ± 0.8 | 130.162104 ± 0.0857894 | |
| | | F3 674.621330 ± 0.424394 | 6.3 ± 0.8 | 128.071847 ± 0.080568 | |
| J0154+4700 2024 Nov 6 | 2.1 | F1 190.727239 ± 0.336841 | 13.8 ± 0.7 | 453.002940 ± 0.800043 | 3.7 |
| | | F2 204.947704 ± 0.229980 | 20.2 ± 0.7 | 421.570958 ± 0.473062 | |
| J0158−2503 2024 Dec 9 | 2.0 | F1 185.471956 ± 1.267393 | 5.4 ± 1.1 | 465.838620 ± 3.183234 | 5.4 |
| | | F2 205.859362 ± 0.229672 | 30.1 ± 1.1 | 419.704011 ± 0.468253 | |
| J0158−2503 2024 Dec 25 | 3.5 | F1 195.827847 ± 0.216539 | 11.5 ± 0.7 | 441.203850 ± 0.487866 | 3.2 |
| | | F2 205.333074 ± 0.054050 | 46.2 ± 0.7 | 420.779752 ± 0.110762 | |
| | | F3 216.696535 ± 0.119549 | 20.9 ± 0.7 | 398.714266 ± 0.219966 | |
| | | F4 411.510990 ± 0.267276 | 9.3 ± 0.7 | 209.957941 ± 0.136367 | |
| | | F5 422.210353 ± 0.349874 | 7.1 ± 0.7 | 204.637332 ± 0.169577 | |
| J0204+8713 2023 Apr 15 | 2.1 | F1 245.025464 ± 1.166706 | 5.0 ± 0.9 | 352.616412 ± 1.679008 | 4.5 |
| | | F2 253.522357 ± 1.170946 | 5.0 ± 0.9 | 340.798346 ± 1.574048 | |
| J0204+8713 2023 Nov 24 | 3.5 | F1 219.381927 ± 0.673149 | 5.5 ± 1.0 | 393.833718 ± 1.208435 | 5.0 |
| | | F2 227.993568 ± 0.634822 | 5.8 ± 1.0 | 378.958059 ± 1.055165 | |
| | | F3 260.311874 ± 0.695208 | 5.3 ± 1.0 | 331.909562 ± 0.886422 | |
| J0204+8713 2023 Dec 30 | 3.3 | F1 266.602480 ± 0.669197 | 6.1 ± 1.0 | 324.078006 ± 0.813466 | 5.2 |
| J0204+8713 2024 Mar 10 | 2.8 | F1 200.571783 ± 1.031661 | 3.5 ± 0.8 | 430.768470 ± 2.215701 | 3.8 |
| | | F2 231.880286 ± 0.560326 | 6.4 ± 0.8 | 372.606061 ± 0.900382 | |
| | | F3 240.743365 ± 0.427515 | 8.4 ± 0.8 | 358.888396 ± 0.637318 | |
| | | F4 245.832988 ± 0.396233 | 9.1 ± 0.8 | 351.458121 ± 0.566479 | |
| J0204+8713 2024 Apr 20 | 2.8 | F1 257.403522 ± 0.753537 | 7.0 ± 1.1 | 335.659743 ± 0.982628 | 5.7 |
| J0634+3848 2024 Dec 9 | 2.0 | F1 839.842921 ± 1.147355 | 1.5 ± 0.3 | 102.876381 ± 0.140545 | 1.3 |
| J0634+3848 2024 Dec 23 | 1.8 | F1 41.138520 ± 0.215606 | 7.9 ± 0.2 | 2100.221398 ± 11.007210 | 1.1 |
| | | F2 488.564003 ± 1.078713 | 1.6 ± 0.2 | 176.844793 ± 0.390460 | |
| | | F3 838.273053 ± 1.143435 | 1.5 ± 0.2 | 103.069041 ± 0.140590 | |
| J0634+3848 2025 Feb 3 | 2.7 | F1 39.988517 ± 0.314764 | 2.8 ± 0.2 | 2160.620260 ± 17.007019 | 0.9 |
| | | F2 489.604041 ± 0.838079 | 1.1 ± 0.2 | 176.469132 ± 0.302071 | |
| | | F3 839.930123 ± 0.687973 | 1.3 ± 0.2 | 102.865700 ± 0.084256 | |
| J0712−1815 2025 Jan 19 | 1.7 | F1 83.947331 ± 1.019242 | 7.1 ± 0.9 | 1029.216760 ± 12.496180 | 4.3 |
| | | F2 151.708404 ± 0.988647 | 7.3 ± 0.9 | 569.513605 ± 3.711383 | |
| | | F3 173.764146 ± 0.444767 | 16.2 ± 0.9 | 497.225705 ± 1.272700 | |
| | | F4 205.496959 ± 0.582887 | 12.4 ± 0.9 | 420.444178 ± 1.192579 | |
| | | F5 256.850678 ± 0.451733 | 16.0 ± 0.9 | 336.382215 ± 0.591608 | |
| J0712−1815 2025 Feb 5 | 2.1 | F1 85.372940 ± 0.888821 | 5.0 ± 0.7 | 1012.030276 ± 10.536287 | 3.2 |
| | | F2 152.917895 ± 0.786854 | 5.6 ± 0.7 | 565.009085 ± 2.907310 | |
| | | F3 170.661015 ± 0.371232 | 12.0 ± 0.7 | 506.266765 ± 1.101262 | |
| | | F4 205.650495 ± 0.317435 | 14.0 ± 0.7 | 420.130280 ± 0.648499 | |
| | | F5 255.632404 ± 0.247233 | 18.0 ± 0.7 | 337.985321 ± 0.326880 | |

**Table 2**
(Continued)

| Observation (UT Date) | Length (hr) | Frequency (cycles per day) | Amplitude (mma) | Period (s) | $4\langle A\rangle$ (mma) |
|---|---|---|---|---|---|
| J0912−2642 2024 Nov 23 | 2.5 | F1 85.319740 ± 0.705133 | 2.3 ± 0.3 | 1012.661314 ± 8.369234 | 1.5 |
| | | F2 91.748870 ± 0.884533 | 1.8 ± 0.3 | 941.700971 ± 9.078756 | |
| J0959−1828 2025 Feb 20 | 1.9 | F1 401.207772 ± 0.785705 | 7.4 ± 0.8 | 215.349766 ± 0.421730 | 4.3 |
| J0959−1828 2025 Mar 28 | 4.1 | F1 402.353479 ± 0.406530 | 0.7 ± 0.1 | 214.736555 ± 0.216966 | 0.4 |
| J1052+1610 2025 Feb 20 | 2.1 | F1 110.100033 ± 0.703626 | 5.0 ± 0.5 | 784.740909 ± 5.015113 | 2.7 |
| | | F2 125.465008 ± 0.736707 | 4.8 ± 0.5 | 688.638222 ± 4.043555 | |
| J1451−2502 2025 Feb 20 | 1.3 | F1 152.394438 ± 1.314322 | 9.4 ± 1.2 | 566.949825 ± 4.889645 | 6.1 |
| | | F2 181.889447 ± 0.515562 | 23.9 ± 1.2 | 475.013814 ± 1.346417 | |
| J1626+2533 2024 May 18 | 2.2 | F1 59.772653 ± 1.110704 | 3.2 ± 0.6 | 1445.477081 ± 26.860062 | 2.9 |
| J1626+2533 2024 Aug 30 | 1.8 | F1 55.157900 ± 0.865205 | 3.6 ± 0.4 | 1566.412064 ± 24.570688 | 2.2 |
| J1722+3958 2024 Aug 8 | | F1 180.570526 ± 0.856759 | 8.1 ± 1.0 | 478.483404 ± 2.270276 | 5.5 |
| | | F2 221.459554 ± 0.603540 | 11.4 ± 1.0 | 390.138960 ± 1.063239 | |
| | | F3 241.467530 ± 0.350202 | 19.7 ± 1.0 | 357.812083 ± 0.518937 | |
| J1929−2926 2024 Aug 8 | 2.1 | F1 201.690586 ± 0.613081 | 10.0 ± 1.0 | 428.378943 ± 1.302148 | 4.7 |
| | | F2 231.051521 ± 0.860352 | 7.2 ± 1.0 | 373.942572 ± 1.392426 | |
| J2026−2254 2024 Jun 14 | 1.4 | F1 173.971069 ± 0.545665 | 35.8 ± 2.1 | 496.634300 ± 1.557707 | 10.3 |
| | | F2 272.089417 ± 0.698970 | 11.5 ± 2.1 | 317.542670 ± 1.982787 | |
| J2208+2059 2024 Aug 30 | 2.0 | F1 139.778117 ± 0.484904 | 5.2 ± 0.4 | 618.122506 ± 2.144328 | 1.9 |
| | | F2 157.468572 ± 0.343530 | 7.4 ± 0.4 | 548.680914 ± 1.196990 | |
| | | F3 182.053632 ± 1.154111 | 2.2 ± 0.4 | 474.585423 ± 3.008587 | |
| | | F4 200.057685 ± 0.658022 | 3.9 ± 0.4 | 431.875436 ± 1.420508 | |

using ULTRACAM and detect a mode at 402.4 ± 0.4 c day$^{-1}$ in the ULTRACAM $g$-band data, though the amplitude has gone down an order of magnitude. Thanks to ULTRACAM's higher cadence and sensitivity, this mode with 0.7 ± 0.1 mma is detected significantly above the noise level in the Fourier transform. While we also have $u$- and $r$-band data from ULTRACAM, the $u$-band data is noisier, and the pulsations have smaller amplitudes in the red. We do not detect any significant frequencies in the $u$- or $r$-band, which is not surprising as the $g$-band data only shows low level variability.

We also observed this white dwarf at GTC. Figure 7 shows the light curves and Fourier transforms. This data further confirms that J0959−1828 is pulsating with significant modes at 404.5 and 430.2 c day$^{-1}$. The former has 1.3 mma in the $g$-band, which goes up to 5.5 mma in the $u$-band. In addition, the second mode at 430.2 c day$^{-1}$ is clearly detected in multiple filters, with the highest amplitude measured in the $u$-band with 2.3 ± 0.3 mma.

In both the data from APO and GTC, there is a low frequency peak, that we tentatively identify as likely real. At APO the peak has a period of 3733.5 s, and at the GTC the peak is at 3421.0 s. These periods are too long to be due to pulsations in DA white dwarfs and no ZZ Ceti exhibits such long pulsation periods. This peak may indicate variability due to rotation, but further observations are required in order to confirm and constrain the source of this peak.

With confirmation of multiperiodic pulsations in this system, J0959−1828 becomes the most massive pulsating white dwarf currently known, though its mass is consistent with the previous record holder J0049−2525 within 1σ. J0959−1828 is just slightly more massive and about 1000 K cooler.

The variability in J0959−1828 is observed at a much lower level compared to J0049−2525, making the detection and confirmation of its pulsation modes more challenging.

### 3.5. J1106+1802

This white dwarf has $M = 1.131 ± 0.011 M_\odot$ and $T_{\rm eff} = 12{,}877 ± 269$ K. It was previously reported as a ZZ Ceti by J. A. Guidry et al. (2021). Their observations revealed three modes at 369.7, 537.2, and 1180.2 s with amplitudes of 10.2%, 0.5%, and 0.6%, respectively.

We observed J1106+1802 on two nights using HiPER-CAM. We include all five bands of data in Figures 8 and 9, and Table 3. On 2025 January 12, we find four significant modes at 159.2, 234.0, 468.0, and 702.1 c day$^{-1}$ that are visible in all filters. However, the last two are clearly harmonics (twice and thrice the frequency) of the dominant mode at 234.0 c day$^{-1}$, which has an amplitude of ≈100 mma in the $u$-band and ≈50 mma in the $g$-band. The second night of GTC observations on 2025 January 19 reveals six pulsation modes with frequencies 161.3, 173.4, 234.2, 295.0, 468.0, and 702.1 c day$^{-1}$ in the $g$-band. The mode at 234.2 c day$^{-1}$ has the highest amplitude again at 49.6 mma, and the latter two modes are clearly its harmonics. The peak at ≈234 c day$^{-1}$ seems to be dominant in all of the data presented here and in J. A. Guidry et al. (2021).

### 3.6. J1626+2533

J1626+2533 was previously classified as an NOV by O. Vincent et al. (2020), where they ruled out variability at the ⩾5.8% level. It has $M = 1.140 ± 0.007 M_\odot$ and $T_{\rm eff} = 13{,}202 ± 189$ K.

**Table 3**
Observation Details and Significant Frequencies for the Pulsators from GTC

| Observation (UT Date & Band) | Length (hrs) | Frequency (cycles per day) | Amplitude (mma) | Period (s) | 4⟨A⟩ (mma) |
|---|---|---|---|---|---|
| J0039−0357 2024 Nov 11 u-band | 4.0 | F1 319.445760 ± 0.354900 | 4.1 ± 0.4 | 270.468451 ± 0.300487 | 2.3 |
| | | F2 331.132800 ± 0.092425 | 15.6 ± 0.4 | 260.922506 ± 0.072828 | |
| | | F3 657.770584 ± 0.528995 | 2.7 ± 0.4 | 131.352788 ± 0.105334 | |
| J0039−0357 2024 Nov 11 g-band | 4.0 | F1 319.221015 ± 0.343340 | 4.6 ± 0.5 | 270.658873 ± 0.327714 | 2.7 |
| | | F2 330.899833 ± 0.076044 | 20.7 ± 0.5 | 261.106206 ± 0.060005 | |
| | | F3 658.206184 ± 0.402211 | 3.9 ± 0.5 | 131.265859 ± 0.080213 | |
| J0039−0357 2024 Nov 11 r-band | 4.0 | F1 319.366661 ± 0.394019 | 2.0 ± 0.2 | 270.535440 ± 0.333773 | 1.2 |
| | | F2 331.321595 ± 0.122158 | 6.6 ± 0.2 | 260.773826 ± 0.096147 | |
| J0039−0357 2024 Nov 11 i-band | 4.0 | F1 320.355050 ± 0.576934 | 1.1 ± 0.2 | 269.700759 ± 0.485710 | 1.0 |
| | | F2 330.937644 ± 0.213182 | 3.0 ± 0.2 | 261.076374 ± 0.168179 | |
| J0039−0357 2024 Nov 11 z-band | 4.0 | F1 331.538544 ± 0.347016 | 1.9 ± 0.2 | 260.603183 ± 0.272769 | 1.0 |
| J0204+8713 2024 Oct 24 u-band | 2.8 | F1 229.049997 ± 0.549858 | 2.4 ± 0.3 | 377.210221 ± 0.905532 | 1.4 |
| | | F2 241.229508 ± 0.401153 | 3.3 ± 0.3 | 358.165138 ± 0.595611 | |
| | | F3 263.272892 ± 0.527690 | 2.5 ± 0.3 | 328.176590 ± 0.657779 | |
| J0204+8713 2024 Oct 24 g-band | 2.8 | F1 210.070146 ± 0.367653 | 3.4 ± 0.3 | 411.291188 ± 0.719819 | 1.9 |
| | | F2 228.423821 ± 0.343547 | 3.6 ± 0.3 | 378.244264 ± 0.568875 | |
| | | F3 240.453547 ± 0.209675 | 5.9 ± 0.3 | 359.320963 ± 0.313327 | |
| | | F4 261.344304 ± 0.309773 | 4.0 ± 0.3 | 330.598367 ± 0.391860 | |
| J0204+8713 2024 Oct 24 r-band | 2.8 | F1 209.669235 ± 0.459851 | 4.0 ± 0.4 | 412.077623 ± 0.903777 | 2.2 |
| | | F2 241.269079 ± 0.305188 | 5.5 ± 0.4 | 358.106395 ± 0.452979 | |
| | | F3 227.177256 ± 0.533518 | 3.1 ± 0.4 | 380.319762 ± .893168 | |
| | | F4 261.766275 ± 0.555513 | 2.9 ± 0.4 | 330.065437 ± 0.700456 | |
| J0204+8713 2024 Oct 24 i-band | 2.8 | F1 209.242210 ± 0.542543 | 1.3 ± 0.2 | 412.918598 ± 1.070654 | 0.9 |
| | | F2 227.604281 ± 0.759877 | 1.0 ± 0.2 | 379.606217 ± 1.267349 | |
| | | F3 241.269079 ± 0.348883 | 2.1 ± 0.2 | 358.106395 ± 0.517834 | |
| | | F4 263.474374 ± 0.502134 | 1.4 ± 0.2 | 327.92563 ± 0.624966 | |
| J0204+8713 2024 Oct 24 z-band | 2.8 | F1 182.377506 ± 0.774661 | 0.7 ± 0.1 | 473.742634 ± 2.012254 | 0.67 |
| | | F2 225.131904 ± 0.832872 | 0.7 ± 0.1 | 383.775016 ± 1.41977 | |
| | | F3 241.532812 ± 0.623171 | 0.9 ± 0.1 | 357.715373 ± 0.922930 | |
| J0959−1828 2025 Jan 28 u-band | 2.0 | F1 405.322396 ± 0.392189 | 5.5 ± 0.3 | 213.163647 ± 0.206257 | 1.7 |
| | | F2 431.073071 ± 0.920288 | 2.3 ± 0.3 | 200.430057 ± 0.427894 | |
| J0959−1828 2025 Jan 28 g-band | 2.0 | F1 404.458573 ± 0.170671 | 1.3 ± 0.03 | 213.618911 ± 0.090142 | 0.2 |
| | | F2 430.181015 ± 0.437800 | 0.5 ± 0.03 | 200.845684 ± 0.204403 | |
| J0959−1828 2025 Jan 28 r-band | 2.0 | F1 403.432286 ± 0.270891 | 2.0 ± 0.1 | 214.162334 ± 0.143803 | 0.5 |
| | | F2 442.490778 ± 0.709953 | 0.8 ± 0.1 | 195.258307 ± 0.313282 | 0.5 |
| J0959−1828 2025 Jan 28 i-band | 2.0 | F1 403.763705 ± 0.406464 | 0.9 ± 0.1 | 213.986544 ± 0.215418 | 0.3 |
| | | F2 430.096437 ± 0.965571 | 0.4 ± 0.1 | 200.88518 ± 0.450989 | |
| J0959−1828 2025 Jan 28 z-band | 2.0 | F1 402.470662 ± 0.984905 | 0.5 ± 0.1 | 214.674033 ± 0.525339 | 0.4 |
| J1106+1802 2025 Jan 12 u-band | 4.0 | F1 159.057435 ± 0.449416 | 9.5 ± 1.3 | 543.200008 ± 1.534809 | 6.2 |
| | | F2 233.947351 ± 0.043353 | 98.7 ± 1.3 | 369.313863 ± 0.068438 | |
| | | F3 468.006138 ± 0.108386 | 39.4 ± 1.3 | 184.612963 ± 0.042755 | |
| | | F4 701.940093 ± 0.278442 | 15.3 ± 1.3 | 123.087427 ± 0.048826 | |
| J1106+1802 2025 Jan 12 g-band | 4.0 | F1 159.218326 ± 0.190364 | 5.2 ± 0.3 | 542.651102 ± 0.648802 | 2.0 |
| | | F2 233.950087 ± 0.020187 | 48.9 ± 0.3 | 369.309544 ± 0.031867 | |
| | | F3 467.959894 ± 0.051295 | 19.2 ± 0.3 | 184.631207 ± 0.020238 | |
| | | F4 702.105212 ± 0.123871 | 8.0 ± 0.3 | 123.05848 ± 0.021711 | |
| J1106+1802 2025 Jan 12 r-band | 4.0 | F1 159.133772 ± 0.248271 | 2.7 ± 0.2 | 542.939433 ± 0.847062 | 1.0 |
| | | F2 233.964876 ± 0.026701 | 24.7 ± 0.2 | 369.286200 ± 0.042144 | |
| | | F3 467.976975 ± 0.070249 | 9.4 ± 0.2 | 184.624468 ± 0.027714 | |
| | | F4 702.164688 ± 0.178092 | 3.7 ± 0.2 | 123.048056 ± 0.031209 | |

**Table 3**
(Continued)

| Observation (UT Date & Band) | Length (hrs) | Frequency (cycles per day) | Amplitude (mma) | Period (s) | $4\langle A\rangle$ (mma) |
|---|---|---|---|---|---|
| J1106+1802 2025 Jan 12 i-band | 4.0 | F1 159.319339 ± 0.299202 | 1.6 ± 0.1 | 542.307045 ± 1.018454 | 0.8 |
| | | F2 233.902946 ± 0.031397 | 15.5 ±0.1 | 369.383975 ± 0.049583 | |
| | | F3 468.043623 ± 0.084273 | 5.8 ± 0.1 | 184.598178 ± 0.033238 | |
| | | F4 702.145067 ± 0.207335 | 2.3 ± 0.1 | 123.051495 ± 0.036336 | |
| J1106+1802 2025 Jan 12 z-band | 4.0 | F1 159.347339 ± 0.496017 | 1.0 ± 0.2 | 542.211753 ± 1.687799 | 0.8 |
| | | F2 233.912839 ± 0.049589 | 10.4 ± 0.2 | 369.368353 ± 0.078305 | |
| | | F3 467.785212 ± 0.126927 | 4.1 ± 0.2 | 184.700153 ± 0.050116 | |
| | | F4 701.797556 ± 0.316585 | 1.6 ± 0.2 | 123.112426 ± 0.055537 | |
| J1106+1802 2025 Jan 19 u-band | 4.0 | F1 161.107075 ± 0.373447 | 14.2 ± 1.6 | 536.289297 ± 1.243121 | 6.8 |
| | | F2 173.408466 ± 0.417985 | 12.8 ± 1.6 | 498.24557 ± 1.200975 | |
| | | F3 234.170136 ± 0.050900 | 101.2 ± 1.5 | 368.962505 ± 0.080199 | |
| | | F4 294.806456 ± 0.364521 | 14.1 ± 1.5 | 293.073636 ± 0.362378 | |
| | | F5 468.012829 ± 0.133153 | 38.4 ± 1.5 | 184.610324 ± 0.052523 | |
| | | F6 702.047175 ± 0.331008 | 15.4 ± 1.5 | 123.068653 ± 0.058026 | |
| J1106+1802 2025 Jan 19 g-band | 4.0 | F1 161.320482 ± 0.164128 | 6.8 ± 0.3 | 535.579853 ± 0.544901 | 2.1 |
| | | F2 173.406241 ± 0.175441 | 6.3 ± 0.3 | 498.251963 ± 0.504098 | |
| | | F3 234.157626 ± 0.022331 | 49.6 ± 0.3 | 368.982217 ± 0.035189 | |
| | | F4 295.041665 ± 0.162018 | 6.8 ± 0.3 | 292.839996 ± 0.160809 | |
| | | F5 467.985148 ± 0.060464 | 18.3 ± 0.3 | 184.621244 ± 0.023853 | |
| | | F6 702.052278 ± 0.146153 | 7.6 ± 0.3 | 123.067758 ± 0.025620 | |
| J1106+1802 2025 Jan 19 r-band | 4.0 | F1 161.201335 ± 0.226324 | 3.4 ± 0.2 | 535.975710 ± 0.752501 | 1.1 |
| | | F2 173.409968 ± 0.246289 | 3.2 ± 0.2 | 498.241255 ± 0.707637 | |
| | | F3 234.171916 ± 0.031167 | 25.0 ± 0.2 | 368.959701 ± 0.049107 | |
| | | F4 294.944749 ± 0.220718 | 3.5 ± 0.2 | 292.936220 ± 0.219215 | |
| | | F5 468.017662 ± 0.087305 | 8.9 ± 0.2 | 184.608418 ± 0.034437 | |
| | | F6 702.196743 ± 0.222142 | 3.5 ± 0.2 | 123.042439 ± 0.038925 | |
| J1106+1802 2025 Jan 19 i-band | 4.0 | F1 161.194328 ± 0.221579 | 2.4 ± 0.2 | 535.999009 ± 0.736788 | 0.8 |
| | | F2 173.378494 ± 0.277647 | 1.9 ± 0.2 | 498.331702 ± 0.798025 | |
| | | F3 234.182128 ± 0.034076 | 15.6 ± 0.2 | 368.943611 ± 0.053685 | |
| | | F4 295.044837 ± 0.251900 | 2.1 ± 0.2 | 292.836848 ± 0.250015 | |
| | | F5 467.974379 ± 0.097340 | 5.4 ± 0.2 | 184.625492 ± 0.038403 | |
| | | F6 702.215787 ± 0.237386 | 2.2 ± 0.2 | 123.039102 ± 0.041594 | |
| J1106+1802 2025 Jan 19 z-band | 4.0 | F1 234.158865 ± 0.058860 | 10.5 ± 0.2 | 368.980265 ± 0.092750 | 0.9 |
| | | F2 295.189508 ± 0.438546 | 1.4 ± 0.2 | 292.693330 ± 0.434838 | |
| | | F3 468.050567 ± 0.165373 | 3.8 ± 0.2 | 184.595439 ± 0.065222 | |
| | | F4 702.236774 ± 0.392176 | 1.6 ± 0.2 | 123.035425 ± 0.068711 | |

We observed J1626+2533 on UT 2024 May 18 and detected a significant mode at $59.8 \, \mathrm{c \, day^{-1}}$ with an amplitude of 3.2 mma. On UT 2024 August 30, we detected another significant mode at $55.2 \, \mathrm{c \, day^{-1}}$ with amplitude 3.6 mma. The light curves and Fourier transforms are shown in Figure 10. Hence, we confirm multiperiodic oscillations in J1626+2533 and reclassify it as a pulsating white dwarf. The rest of the newly discovered ZZ Cetis in our sample are presented in Appendix A.

## 4. Nonvariable White Dwarfs

G. Jewett et al. (2024) reported 14 white dwarfs classified as NOVs in their sample based on the literature data. We reobserved five white dwarfs that were previously classified as nonvariable by O. Vincent et al. (2020), including J0408+2323, J0538+3212, J0657+7341, J1243+4805, and J1928+1526. These all lie within the boundaries of the instability strip, yet we also do not detect any significant variations in these systems. In addition, we find 10 additional NOVs among the newly observed systems.

We present the light curves and the corresponding Fourier transforms for the NOVs in Appendix B. We summarize our

APO observations, including the length of observation and $4\langle A\rangle$ significance levels in Table 7 in Appendix B. The detection limits range from 1.5 to 7.7 mma, with a median at 3.1 mma.

None of these objects show any significant modes above the $4\langle A\rangle$ limits. We were able to observe four of these targets on two separate nights at APO, and both nights of data confirm the NOV status for those objects. Furthermore, we were able to observe two of these targets, J0408+2323 and J0657+7341, at GTC using HIPERCAM (see Table 8 in Appendix B), with detection limits down to 0.5 mma in the g-band, and still did not detect any significant variability. Because they fall near or within the ZZ Ceti instability strip, it is somewhat surprising to find so many NOVs in the instability strip.

Note that O. Vincent et al. (2020) found a significant discrepancy between the photometric and spectroscopic temperatures for one of these objects, J1243+4805, where the spectroscopic temperature places it outside of the instability strip. This shows a potential caveat for NOVs close to the edges of the instability strip. O. Vincent et al. (2020) suggested that the photometric temperatures might sometimes
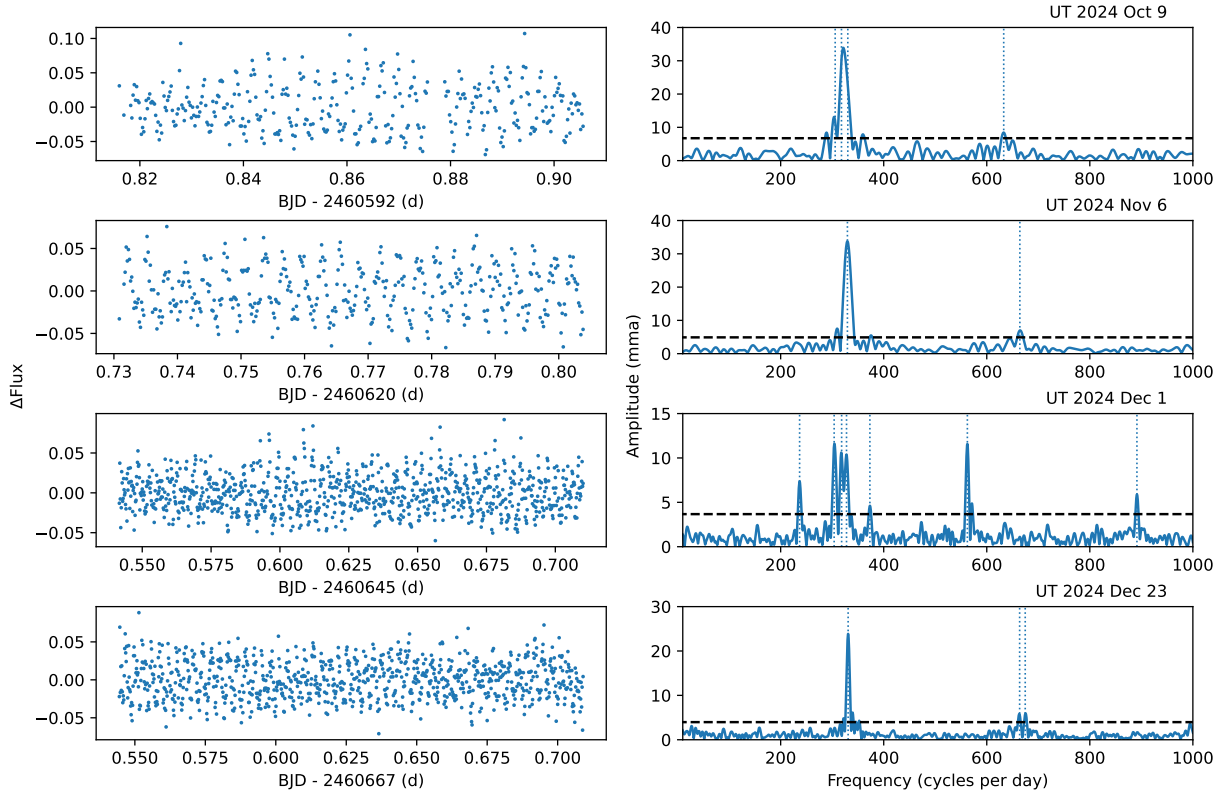
**Figure 2.** Light curves (left) and their Fourier transforms (right panels) for J0039−0357 observed on four different nights. The horizontal black dashed lines indicate 4 times the average amplitude in the Fourier transforms, while the vertical dashed blue lines mark the significant frequencies. Table 2 provides a list of the frequencies detected for each observation.
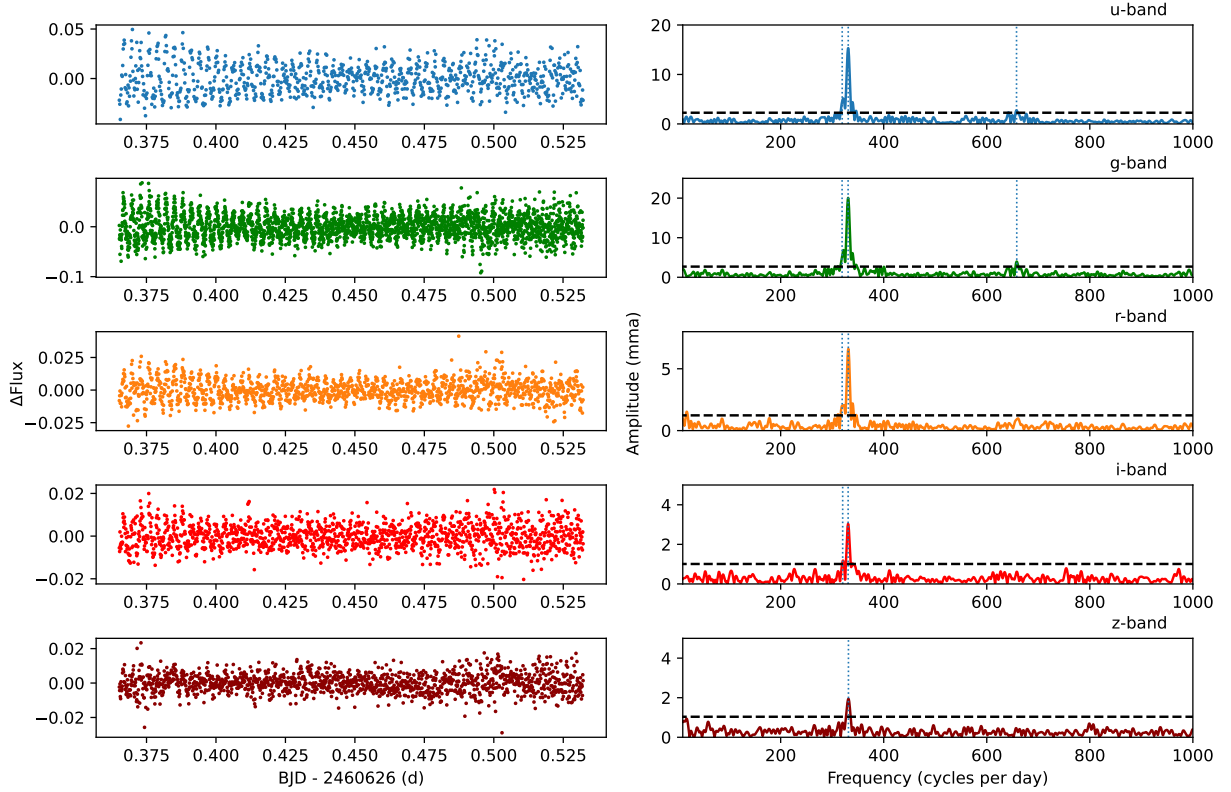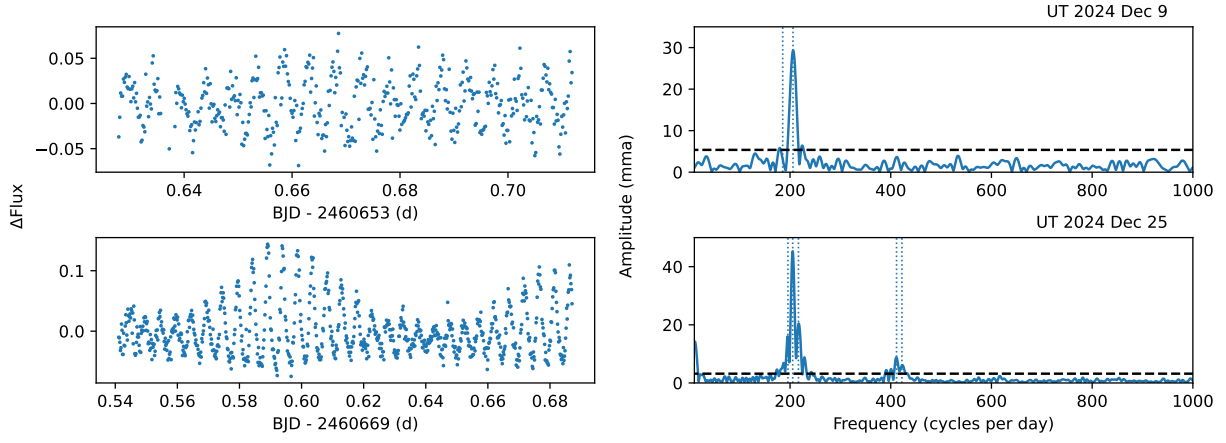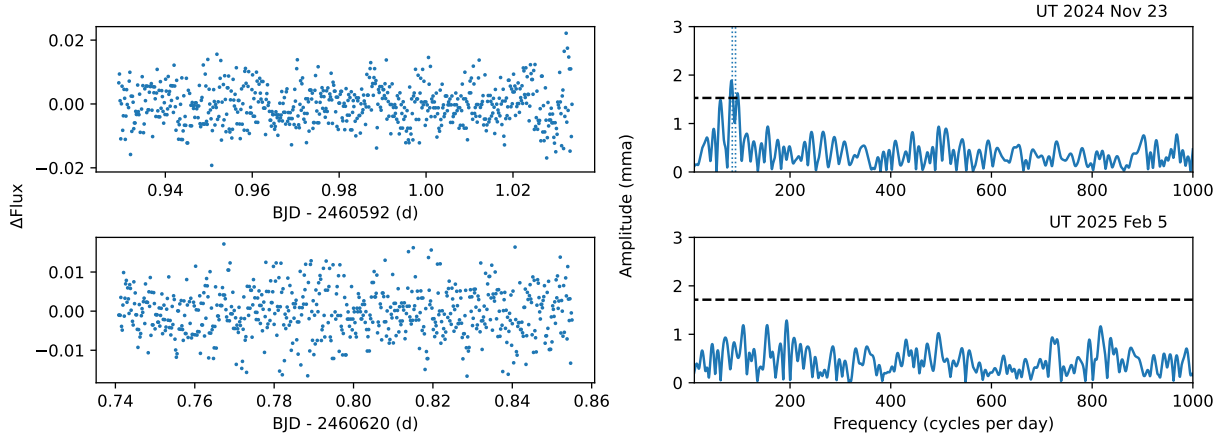


**Figure 3.** Light curves (left) and their Fourier transforms (right panels) for J0039−0357 observed on 2024 November 11 at the GTC using HiPERCAM. The corresponding filter is labeled above the Fourier transform. Table 3 provides a list of the frequencies detected for each observation.

**Figure 4.** Light curves and Fourier transforms for J0158−2503.



**Figure 5.** Light curves and Fourier transforms for J0912−2642.
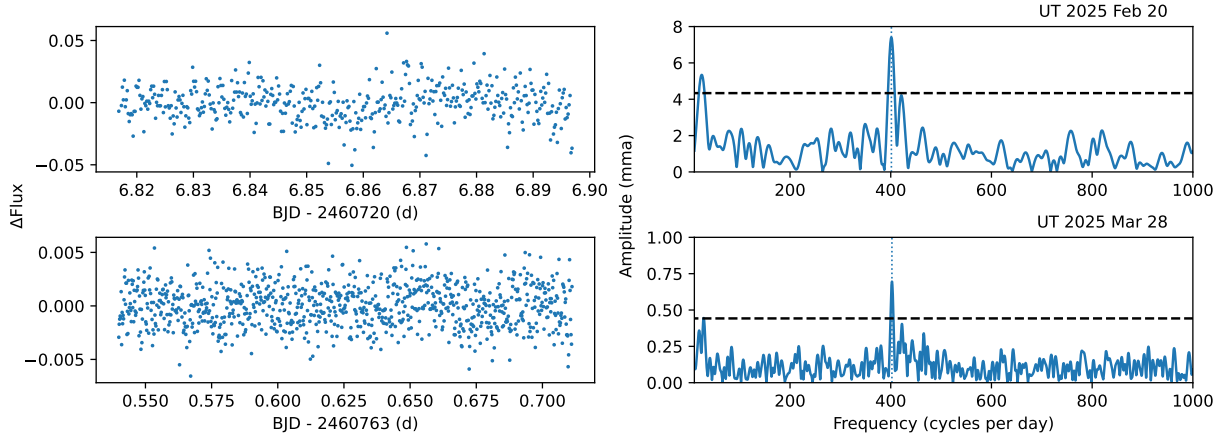


**Figure 6.** Light curves and Fourier transforms for J0959−1828. The top and bottom rows show data taken at APO and NTT/ULTRACAM (g-band), respectively.

be underestimated. We discuss the purity of the instability strip in Section 5.4 and discuss other potential reasons for why we are finding a relatively large number of NOVs in the instability strip for massive white dwarfs.

## 5. Discussion

### 5.1. Trends: Period versus Temperature

As a DA white dwarf cools, it is predicted to start pulsating when it is cool enough to have a hydrogen partial ionization zone deep enough to excite global pulsations. With further

cooling, the base of the partial ionization zone moves deeper and the thermal timescale increases, which leads to the excitation of modes with longer pulsation periods (M. H. Montgomery 2005; A. S. Mukadam et al. 2006). In addition, the total pulsation power is expected to increase with increasing mass of the partial ionization zone.

J. C. Clemens (1993) found a trend between the weighted mean period (WMP), where each period is weighted by the corresponding amplitude, and the effective temperature of a dozen pulsating, average mass DAV white dwarfs: hotter stars have the shortest periods, and the pulsation periods lengthen
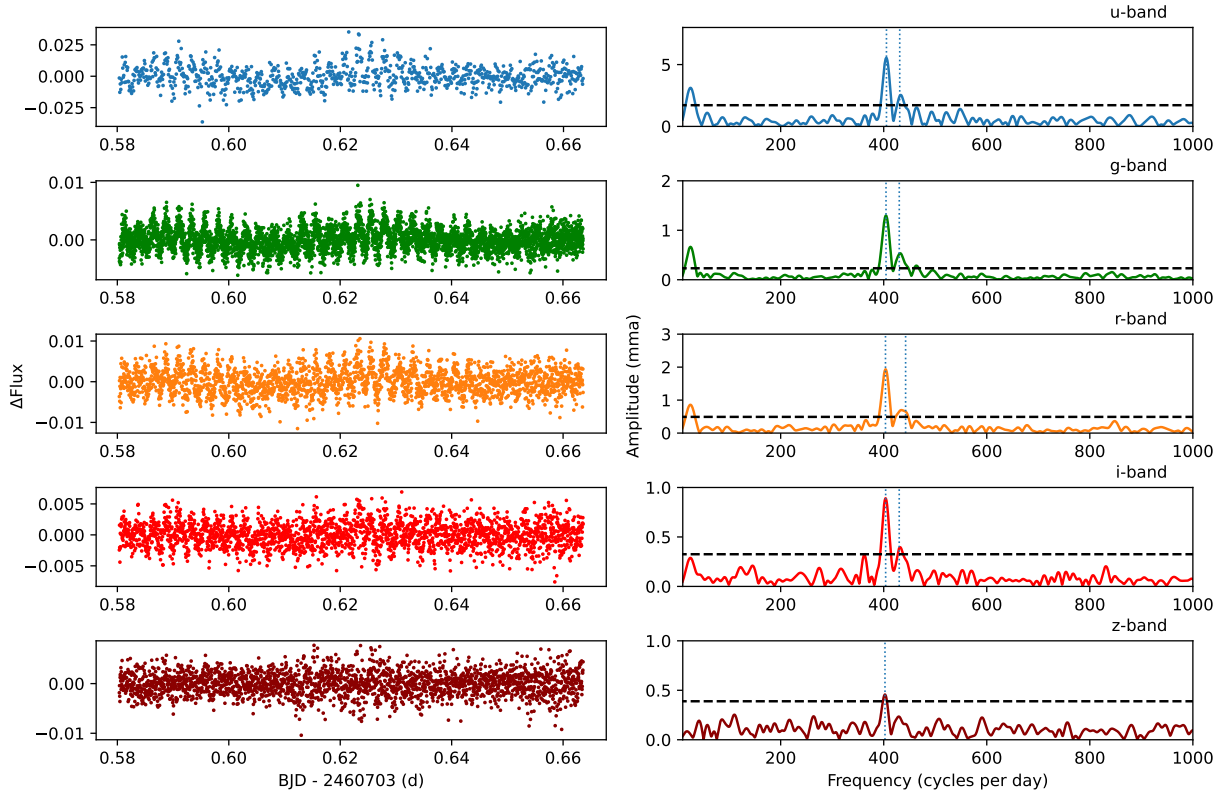
**Figure 7.** Light curves and Fourier transforms for J0959−1828 taken at GTC.
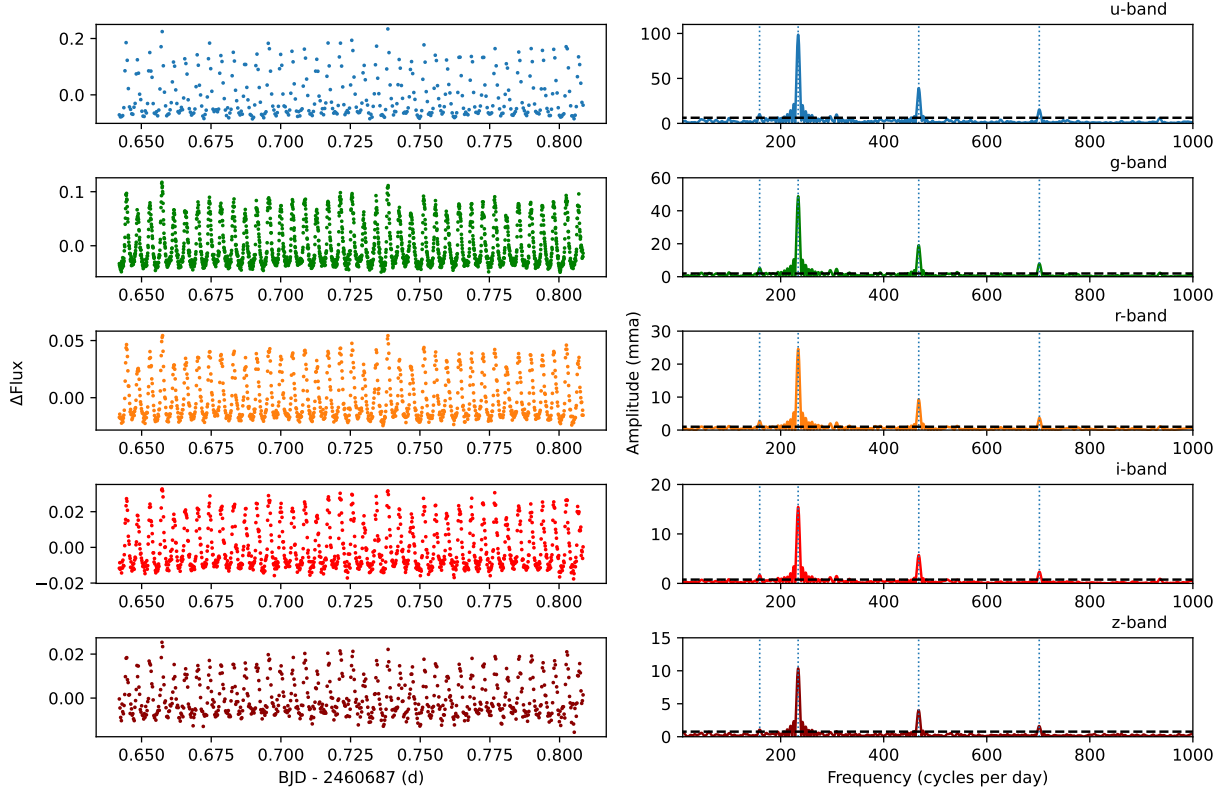


**Figure 8.** Light curves and Fourier transforms for J1106+1802 taken on 2025 January 12.

by an order of magnitude from the blue edge to the red edge of the instability strip. J. C. Clemens (1993) also detected a three orders of magnitude increase in the total pulsation power over the same temperature and frequency range. The same trends were confirmed with larger samples of average mass DAVs by A. Kanaan et al. (2002) and A. S. Mukadam et al. (2006).
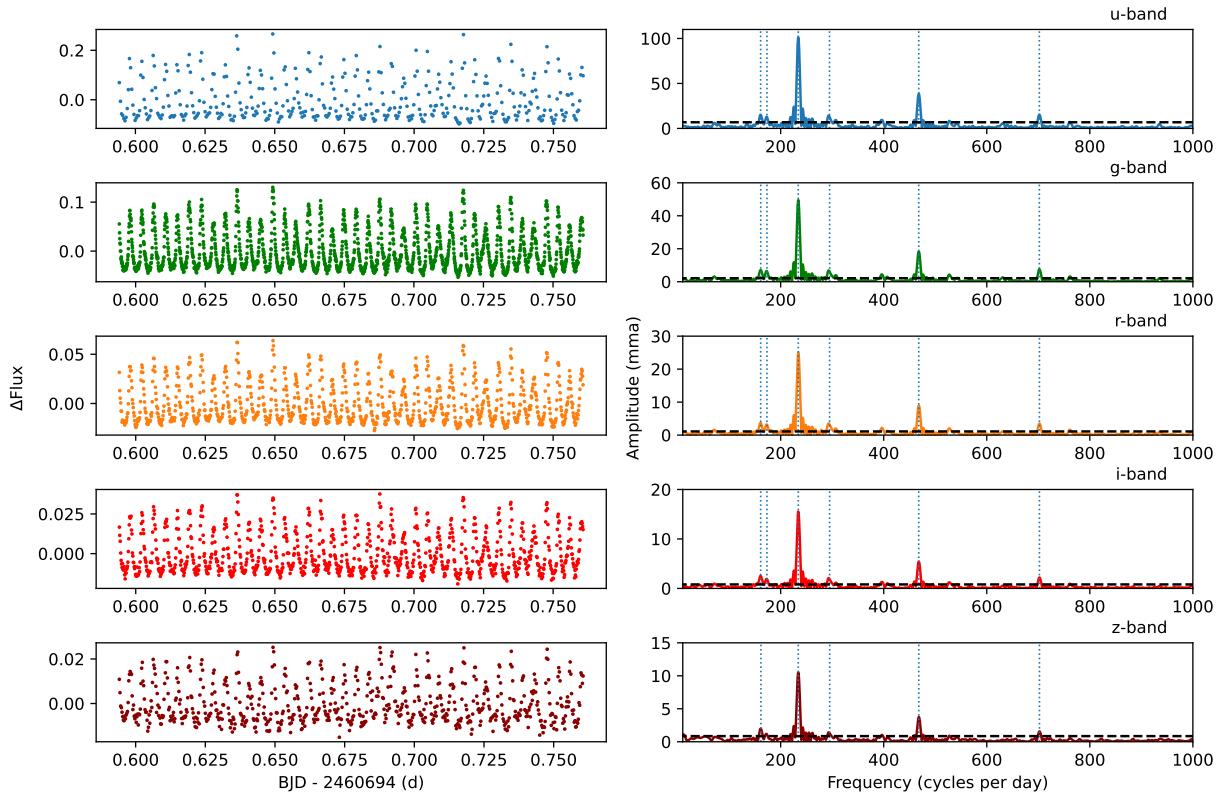
**Figure 9.** Light curves and Fourier transforms for J1106+1802 taken on 2025 January 19.
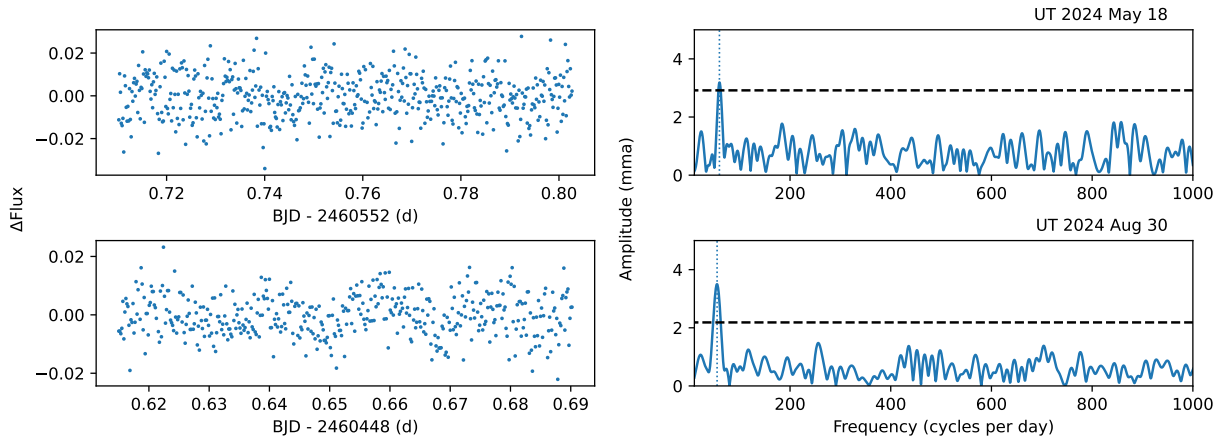


**Figure 10.** Light curves and Fourier transforms for J1626+2533.

Figure 11 shows the WMP versus effective temperature for our sample of massive DAVs, where the color of the points represent the mass of each object. For targets that were observed on multiple nights, we calculated a single WMP using all of the significant periods from all of the nights, excluding the harmonics and combination frequencies. We include the previously studied ultramassive pulsators BPM 37093, GD 518, and J0049−2525 for reference. BPM 37093 is not in the G. Jewett et al. (2024) sample as it lies outside of the Pan-STARRS footprint. Table 4 lists the WMPs for each star.

As in previous studies that looked into the relation between the WMP and effective temperature for average mass white dwarfs mentioned above, Figure 11 reveals a clear trend between the WMP and $T_{\rm eff}$ for massive DAVs: WMP increases with decreasing effective temperature. This is mainly because the convection zone deepens into the star. Note also that the cooling of white dwarfs induces an intrinsic lengthening of the pulsation periods, because the core is increasingly degenerate and the Brunt–Väisälä frequency is smaller (Equation (34) in M. Tassoul et al. 1990). Finally, cooler white dwarfs of a given mass have a more crystallized core where $g$ modes cannot propagate (M. H. Montgomery & D. E. Winget 1999), which leads to a smaller propagation region and further lengthening of the period spacing and the periods themselves (see Equations (43) and (44) in M. Tassoul et al. 1990) as clearly depicted in Figure 6 of F. C. De Gerónimo et al. (2019). The dashed line of Figure 11 shows a linear fit to the data for comparison. Note that we are not claiming a linear relation between WMP and $T_{\rm eff}$ (see, for example, J. C. Clemens 1993), this line is simply used to guide the eye. The previously known ultramassive DAVs, BPM 37093, GD 518, and J0049−2525, all follow this trend as well.

12
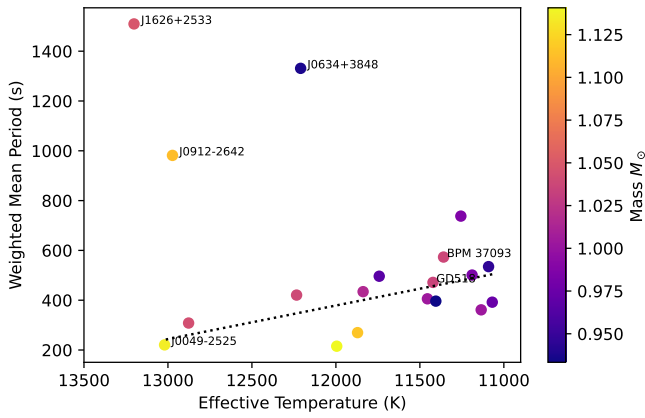
**Figure 11.** Weighted mean period vs. effective temperature for the ZZ Ceti white dwarfs in our sample. The color of the point indicates the mass of each star. We include the well-known ultramassive ZZ Cetis BPM 37093, GD 518, and J0049−2525 for reference. The dashed black line shows the best-fitting line to the data, excluding the three outliers: J0634+3848, J0912−2642, and J1626+2533, which are labeled.

**Table 4**
Weighted Mean Period (WMP) and Square Root of Total Power

| Object Name | WMP (s) | $\sqrt{\text{Total Power}}$ (mma) |
|---|---|---|
| J0039−0357 | 269.8 | 66.9 |
| J0154+4700 | 434.3 | 24.5 |
| J0158−2503 | 420.6 | 60.3 |
| J0204+8713 | 361.3 | 22.2 |
| J0634+3848 | 1331.1 | 9.0 |
| J0712−1815 | 496.3 | 38.7 |
| J0912−2642 | 981.5 | 2.9 |
| J0959−1828 | 214.4 | 7.4 |
| J1052+1610 | 737.7 | 6.9 |
| J1106+1802 | 308.3 | 24.3 |
| J1451−2502 | 501.0 | 25.7 |
| J1626+2533 | 1509.5 | 4.8 |
| J1722+3958 | 392.1 | 24.2 |
| J1929−2926 | 405.6 | 12.3 |
| J2026−2254 | 396.3 | 37.6 |
| J2208+2059 | 534.9 | 10.1 |

A striking revelation in Figure 11 is that there are three outliers: J0634+3848, J0912−2642, and J1626+2533, which are labeled on the plot. J1626+2533 is the hottest variable in our sample, yet it has the longest WMP, which is the exact opposite of the visible trend in this diagram. J1626+2533 was observed on two different nights, with each night of data revealing only one significant mode, but those modes have periods differing by $>3\sigma$. Hence, they are unlikely to be from rotation. The multiperiodic variability demonstrates that J1626 +2533 is a pulsator. It is possible that the relatively long period oscillations observed so far in this system with periods of 1445.5 and 1566.4 s only represent part of the power spectrum of this object, and additional time-series photometry is required to understand its nature. Further support for this comes from another outlier, J0634+3848, which shows both short period and long period variability. The photometric data for J0634+3848, see Figure 19 in Appendix A, reveals variability at both ∼100 and ∼2100 s. Since the latter have larger amplitudes, they dominate the WMP measurement. Hence, it is likely that our WMP measurement may not represent the actual period distribution in this star.

The last outlier visible in Figure 11, J0912−2642, is a bit of a mystery. We were only able to detect multiperiodic variations (two modes) with amplitudes ∼2 mma in this star once, but we only have two nights of observations. It is possible that the relatively low amplitudes seen in this ultramassive white dwarf are similar to J0959−1828, and that this white dwarf also requires additional observations to confirm the pulsation modes and constrain its WMP accurately.

### 5.2. Trends: Period versus Mass

Theoretical models predict a dramatic change in pulsation periods with mass. The larger the mass, the higher the gravity, and therefore the higher the Brunt–Väisälä frequency, see Equation (34) in M. Tassoul et al. (1990). This shifts the entire spectrum of g-mode periods toward shorter periods. The predicted trend can be seen, for instance, in Figure 9 in P. A. Bradley (1996) for ZZ Ceti stars, and in Figure 6 in F. C. De Gerónimo et al. (2019) for ultramassive ZZ Ceti stars. Hence, periods and period spacings are expected to decrease with increasing mass.

A comparison between the pulsation periods for extremely low-mass (ELM) and average mass DAVs shows that the variability timescale is significantly longer for ELM white dwarfs (J. J. Hermes et al. 2013). For example, the ELM white dwarf companion to the millisecond pulsar PSR J1738+0333 shows pulsation modes with periods ranging from about 1800 to 4980 s, and potentially to even longer periods (M. Kilic et al. 2018). Besides this comparison between ELM white dwarfs and average mass DAVs, we have not been able to find an observational study of the correlation between mass and pulsation period for large samples of pulsating white dwarfs in the literature.

For ultramassive white dwarfs, crystallization also needs to be considered because for a given effective temperature, the crystallized mass fraction in the core is larger for higher masses. Since g modes cannot propagate through the crystallized regions, this reduces the region where the g modes can propagate. Therefore, for massive white dwarfs with crystallized cores and a reduced g-mode propagation zone, period spacing is larger and periods tend to become longer, see Equations (43) and (44) in M. Tassoul et al. (1990) and Figure 6 of F. C. De Gerónimo et al. (2019). Crystallization has the opposite effect of a larger Brunt–Väisälä frequency, but the latter is dominant and the overall expectation is that high mass white dwarfs should display shorter pulsation periods.

Figure 12 shows the WMP versus mass for our massive pulsating DAV sample. The dashed line shows a linear fit to the data to guide the eye. As expected from the pulsation models, the WMP indeed decreases with increasing mass, from about 600 s for $0.9\,M_\odot$ white dwarfs to ∼200 s for the most massive pulsators at $1.3\,M_\odot$. This is a nice confirmation of the predicted trend with mass for massive ZZ Ceti white dwarfs. Not surprisingly, the three outliers in the WMP versus $T_{\rm eff}$ plane, J0634+3848, J0912−2642, and J1626+2533, are also outliers in this diagram. But the three previously studied ultramassive pulsators, BPM 37093, GD 518, and J0049 −2525, fall in nicely with our sample. In fact, the WMP of J0049−2525 is very close to the newly confirmed ultramassive pulsator J0959−1828.
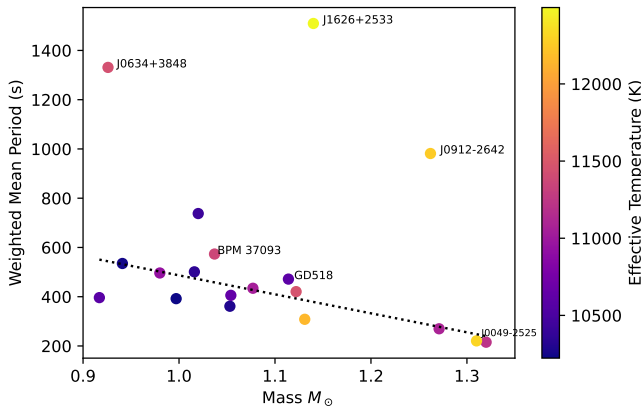
**Figure 12.** Weighted mean period vs. mass for the ZZ Ceti white dwarfs in our sample. The color of the points are representative of the effective temperature of the star. The dashed black line shows the best-fitting line to the data, excluding the three outliers.
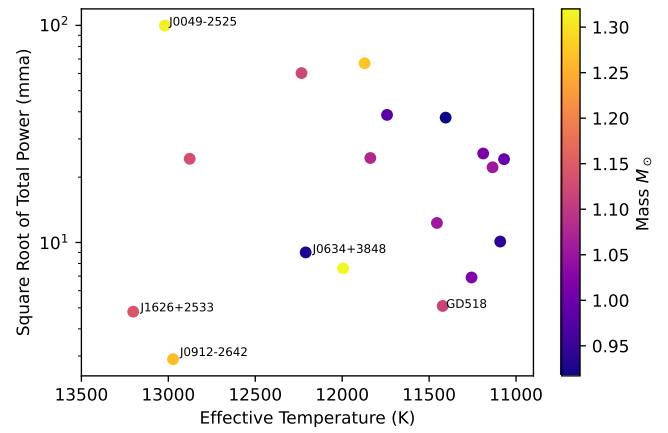


**Figure 13.** Square root of the total power vs. effective temperature for the observed pulsators in our sample plus GD 518 and J0049−2525. The *y*-axis is set to a log scale, and the color of the points are indicative of the white dwarf's mass. The three outliers from Figure 11 are also labeled.

### 5.3. Trends: Period versus Power

Studying a sample of ∼100 average mass DAVs, A. S. Mukadam et al. (2006) found a correlation between the square root of total power[13] versus effective temperature or WMP, since WMP is correlated with $T_{\rm eff}$ (also see J. C. Clemens 1993). They found that once the pulsations set in at the blue edge of the instability strip, the total power increases with decreasing temperature, reaches a maximum in the middle of the instability strip (around WMP ∼800 s), and then declines near the red edge, just before the pulsations shut down.

Figure 13 shows the square root of the total power versus effective temperature for our sample of massive DAV white dwarfs, with each point's color corresponding to its mass. Table 4 lists the square root of the total power for each star for reference. Our sample is much smaller than the one presented in A. S. Mukadam et al. (2006), but we confirm the overall trend seen in average mass DAVs. The pulsators in the middle of the instability strip on average show pulsations with the highest power, and the total power clearly decreases toward the red edge.

The blue edge of the instability strip is more complicated. Even though J0049−2525 is one of the hottest pulsators in our sample, it shows the highest total power, but it is also one of the most massive pulsators known with a significantly crystallized core (M. Kilic et al. 2023a; O. Caliskan et al. 2025). On the other hand, the two other objects near the blue edge, J0912−2642 and J1626+2533, have significantly lower total power, which would be more in line with lower amplitudes expected near the blue edge. However, these two stars are also outliers in Figure 11. Hence, we cannot constrain the overall trend in total power for this massive white dwarf sample without additional follow-up observations to constrain the nature of these outliers.

### 5.4. The Purity of the ZZ Ceti Strip

Figure 14 shows the pulsators (green) and NOVs (red points) in the MWDD 100 pc sample along with the empirical boundaries of the photometric instability strip from O. Vincent et al. (2020). The four most massive pulsators are labeled. This plot of the massive MWDD 100 pc sample shows a much more complete picture of the massive and ultramassive pulsators

compared to the one presented in G. Jewett et al. (2024), as now every white dwarf that is near or within the boundaries of the instability strip has time-series photometry available. For reference, the most massive white dwarf on this plot is J1140+2322, which was classified as a NOV by M. Kilic et al. (2023b). A summary of the newly identified and previously known pulsators and NOVs can be found in Table 5.

There is a large number of NOVs within the instability strip. It is possible that the slope of the red edge could be slightly different, which could help remove some of the offending NOVs from the sample. However, we do not try to adjust this boundary based on our observations, since observations of additional white dwarfs lying outside of the strip would be necessary to determine the exact location of the red edge for these massive white dwarfs.

The purity of the ZZ Ceti instability strip has been studied extensively in the literature. If it is pure, if every star in the instability strip shows pulsations, this would indicate that this is an evolutionary phase that every DA white dwarf goes through. Hence, we can use the internal structures derived through asteroseismology, such as constraints on the surface H layer thickness, to the entire population of DA white dwarfs. In addition, if the strip is pure, it also enables identification of additional pulsators solely through measurements of their atmospheric parameters (A. Gianninas et al. 2005).

In their search for DAV white dwarfs within the SDSS spectroscopy sample, A. S. Mukadam et al. (2004) found several nonvariables within the instability strip and questioned its purity. B. G. Castanheira et al. (2007) followed up two of these nonvariables and found them to show low-amplitude variability that escaped detection in earlier observations. They suggested that the ZZ Ceti strip is likely pure, but also highlighted other NOVs that needed to be observed. P. Bergeron et al. (2004) found that the spectroscopic method for estimating the atmospheric parameters had a 100% success rate for predicting which stars should pulsate. Their analysis found no NOVs within the ZZ Ceti strip, supporting the idea that the instability strip is pure and that all DA white dwarfs evolve through this phase.

We find answering the question of whether all DA white dwarfs evolve through the ZZ Ceti phase irrelevant. Obviously, all white dwarfs will pass through the instability strip as they cool. The actual question is what are the potential

---

[13] Total power is defined as the sum of the amplitudes squared.
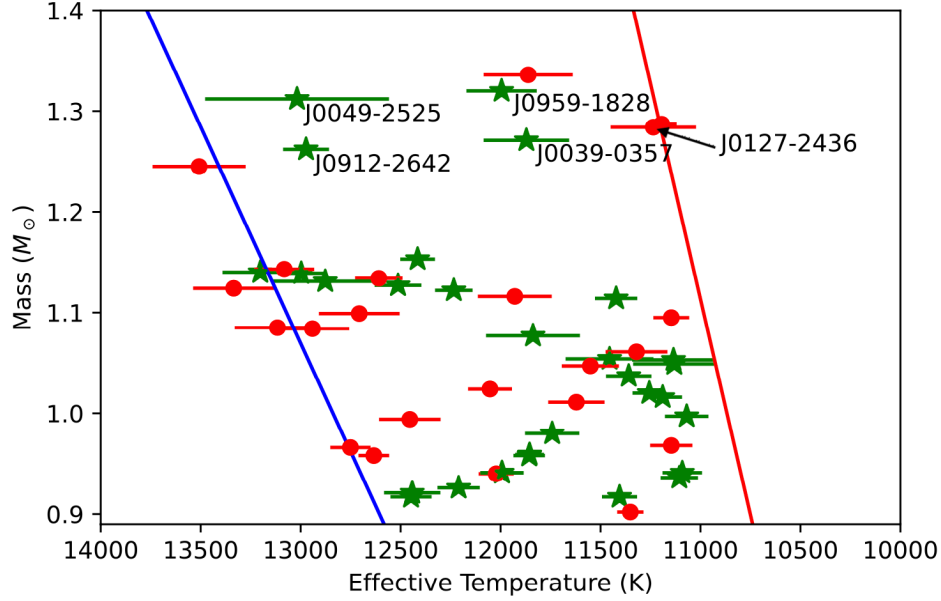
**Figure 14.** Masses and effective temperatures for our follow-up sample of massive DA white dwarf sample including white dwarfs from this work and those previously known in the literature and the four most massive pulsators labeled and J0127−2436, which lies on the edge of the instability strip. The objects marked with by a red point are NOVs. The green stars mark the pulsators. The blue and red lines show the empirical boundaries of the photometric ZZ Ceti instability strip from O. Vincent et al. (2020).

**Table 5**
Massive and Ultramassive Pulsators and NOVs in MWDD 100 pc Sample

| Pulsators | Mass ($M_\odot$) | References | NOVs | Mass ($M_\odot$) | References |
|---|---|---|---|---|---|
| J0039−0357 | $1.271 \pm 0.009$ | This Work | J0050−2826 | $1.061 \pm 0.011$ | This Work |
| J0049−2525 | $1.312 \pm 0.010$ | M. Kilic et al. (2023a) | J0127−2436 | $1.284 \pm 0.009$ | This Work |
| J0135+5722 | $1.153 \pm 0.004$ | F. C. De Gerónimo et al. (2025) | J0135+5722 | $1.153 \pm 0.004$ | O. Vincent et al. (2020) |
| J0154+4700 | $1.077 \pm 0.014$ | This Work | J0234−0511 | $0.958 \pm 0.004$ | A. Gianninas et al. (2011) |
| J0158−2503 | $1.122 \pm 0.007$ | This Work | J0347−1802 | $1.143 \pm 0.007$ | J. A. Guidry et al. (2021) |
| J0204+8713 | $1.053 \pm 0.015$ | O. Vincent et al. (2020), G. Jewett et al. (2024) and This Work | J0408+2323 | $1.024 \pm 0.008$ | O. Vincent et al. (2020) and This Work |
| J0448−1053 | $0.941 \pm 0.007$ | A. D. Romero et al. (2022) | J0538+3212 | $0.994 \pm 0.010$ | O. Vincent et al. (2020) and This Work |
| J0551+4135 | $1.139 \pm 0.005$ | O. Vincent et al. (2020) and M. Uzundag et al. (2025, submitted) | J0634+3848 | $0.926 \pm 0.006$ | O. Vincent et al. (2020) |
| J0634+3848 | $0.926 \pm 0.006$ | This Work | J0657+7341 | $1.134 \pm 0.007$ | O. Vincent et al. (2020) and This Work |
| J0712−1815 | $0.980 \pm 0.008$ | This Work | J0725+0411 | $0.940 \pm 0.008$ | This Work |
| J0856+6206 | $0.958 \pm 0.007$ | O. Vincent et al. (2020) | J0949−0730 | $1.084 \pm 0.008$ | This Work |
| J0912−2642 | $1.262 \pm 0.002$ | This Work | J0950−2841 | $1.124 \pm 0.006$ | This Work |
| J0959−1828 | $1.320 \pm 0.004$ | This Work | J1140+2322 | $1.336 \pm 0.006$ | M. Kilic et al. (2023b) |
| J1052+1610 | $1.020 \pm 0.009$ | This Work | J1243+4805 | $0.966 \pm 0.006$ | O. Vincent et al. (2020) and This Work |
| J1106+1802 | $1.131 \pm 0.011$ | J. A. Guidry et al. (2021) and This Work | J1342−1413 | $0.902 \pm 0.006$ | This Work |
| BPM 37093 | $1.037 \pm 0.008$ | A. Kanaan et al. (1992) | J1552+0039 | $1.245 \pm 0.011$ | This Work |
| J1451−2502 | $1.016 \pm 0.011$ | This Work | J1626+2533 | $1.140 \pm 0.007$ | O. Vincent et al. (2020) |
| J1626+2533 | $1.140 \pm 0.007$ | This Work | J1655+2533 | $1.287 \pm 0.002$ | B. Curd et al. (2017) |
| GD 518 | $1.114 \pm 0.006$ | J. J. Hermes et al. (2013) | J1656+5719 | $1.047 \pm 0.010$ | This Work |
| J1722+3958 | $0.997 \pm 0.010$ | This Work | J1813+4427 | $1.095 \pm 0.007$ | O. Vincent et al. (2020) |
| J1812+4321 | $0.921 \pm 0.007$ | A. D. Romero et al. (2022) | J1819+1225 | $1.116 \pm 0.012$ | This Work |
| J1929−2926 | $1.054 \pm 0.016$ | This Work | J1910+7334 | $1.085 \pm 0.008$ | O. Vincent et al. (2020) |
| J2026−2254 | $0.917 \pm 0.008$ | This Work | J1928+1526 | $1.011 \pm 0.012$ | O. Vincent et al. (2020) and This Work |
| J2208+2059 | $0.941 \pm 0.011$ | This Work | J2107+7831 | $1.099 \pm 0.009$ | This Work |

**Note.** Masses from G. Jewett et al. (2024). BPM 37093 mass is from M. W. O'Brien et al. (2024) and is outside of the MWDD 100 pc sample, but it is included for reference.

mechanisms that can stop or hide pulsations in these white dwarfs as they go through the strip? There are several candidates:

1. Magnetic fields have been suggested to suppress pulsations in white dwarfs by affecting atmospheric convection, thus disrupting the driving mechanism of pulsations (see N. Z. Rui et al. (2025) for discussion of suppression directly by the magnetic field). P. E. Tremblay et al. (2015) demonstrated that magnetic fields stronger than about 50 kG are sufficient to suppress convection in white dwarf photospheres, which was later confirmed through observations of WD 2105−820, where only the radiative models can explain the spectral energy distribution of this weakly magnetic white dwarf (N. P. Gentile Fusillo et al. 2017). Hence, magnetism is likely to stop pulsations in DA white dwarfs. Low-resolution spectroscopy is not sensitive to fields below 100 kG for massive DA white dwarfs (M. Kilic et al. 2015). Hence, such weakly magnetic stars would appear as normal DAs, yet would not show pulsations.

S. Bagnulo & J. D. Landstreet (2022) found that average mass white dwarfs are rarely magnetic at birth, but weak fields appear slowly, especially after the stars go through core crystallization. For example, out of the 100 objects with $0.5 < M < 0.8\,M_\odot$ and $T_{\rm eff} \geqslant 10{,}000$ K in their sample, only 4 are magnetic: WD 1105–048 (0.01 MG), WD 1105–340 (0.15 MG), WD 1704+481.1 (0.01 MG), and WD 2047+372 (0.06 MG). Even though magnetism can stop pulsations in white dwarfs, it is rare to find magnetism in average mass white dwarfs while they are going through the ZZ Ceti strip, and therefore we would expect the instability strip to be nearly (∼96%) pure for those most common DAVs.

On the other hand, massive white dwarfs, a large fraction of which are likely merger remnants (K. D. Temmink et al. 2020; G. Jewett et al. 2024), tend to be strongly magnetic at birth. For comparison, out of the 15 objects with $M \geqslant 0.9\,M_\odot$ and $T_{\rm eff} \geqslant 10{,}000$ K in the S. Bagnulo & J. D. Landstreet (2022) sample, 9 are magnetic. Only one of the massive magnetic white dwarfs in that sample, WD 2051–208 ($B = 0.3$ MG) has a field strength lower than 1 MG. A. Gianninas et al. (2011) classified this white dwarf as a DA based on a low-resolution spectrum that covers only up to H$\beta$. Hence, we can assume a one in seven contamination rate of the "apparently" nonmagnetic massive DA sample by weakly magnetic stars like WD 2051–208. Using a binomial distribution, this corresponds to a fraction of $14.3^{+15.1}_{-7.1}\%$. Hence, the ZZ Ceti strip for massive white dwarfs could be contaminated by weakly magnetic DAs where the field strength is not strong enough to cause visible Zeeman split lines in low-resolution spectra obtained by G. Jewett et al. (2024). This could explain some of the NOVs in our sample.

2. Given the relatively low-amplitude pulsations observed in several massive white dwarfs in our sample, our precision may not be sufficient to detect pulsations in all. J0959−1828 is an excellent example, where the pulsation amplitude changed by an order of magnitude over the three nights of observations, and we could confirm pulsations in this system only because of the exquisite data from ULTRACAM and HIPERCAM. Without those additional data, we would not be able to detect the ∼0.7 mma oscillations in this target. Our sensitivity limits for the NOVs presented in Table 7 range from 1.5 to 7.7 mma, whereas the two NOVs observed with HIPERCAM (see Table 8) have detection limits down to 0.5 mma in the $g$-band.

Hence, we cannot rule out low-amplitude pulsations in a significant fraction of the NOVs that we identified.

Based on these arguments, additional time-series observations of the NOVs in our sample would be helpful to search for low-amplitude pulsations and confirm their nature. However, given the relatively large fraction of magnetic white dwarfs among the young and massive white dwarfs in volume-limited samples (S. Bagnulo & J. D. Landstreet 2022; G. Jewett et al. 2024), perhaps it is not surprising that some of these massive white dwarfs are weakly magnetic. Such objects could appear as normal DAs in low-resolution spectra, yet may not show any variability while they go through the ZZ Ceti instability strip.

3. The method in which the physical parameters of the white dwarf are calculated can impact the position of the star in the instability strip, potentially pushing it outside of the bounds. There are two methods that are generally used to estimate the physical parameters of white dwarfs: the spectroscopic and photometric methods. The parameters used in our study are based on the photometric method (G. Jewett et al. 2024). For one of the NOVs in our sample, J1243+4805, O. Vincent et al. (2020) report a spectroscopic temperature of 14,838 K, which is much hotter than the photometric temperature of 12,751 K and would push this NOV beyond the blue edge of the instability strip.

The spectroscopic method requires accurate flux calibration and high signal-to-noise ratio spectra covering the gravity-sensitive higher-order Balmer lines. The available spectra for the majority of our targets do not have sufficient signal-to-noise ratio for such an analysis, but we identify at least five NOV white dwarfs that are outside of the ZZ Ceti strip based on their spectroscopic temperatures. Figure 15 shows our spectroscopic fits to three of these NOVs, where the spectroscopic temperatures are all hotter than 14,000 K, which would push all three stars outside of the instability strip. Either the photometric method is underestimating or the spectroscopic method is overestimating their temperatures by 10%–20%. This is consistent with C. Genest-Beaulieu & P. Bergeron (2019), who found that the spectroscopic temperatures of DA stars exceed the photometric values by ∼10% above 14,000 K likely due to inaccurate treatment of Stark broadening in the model spectra. Other factors affecting the spectroscopic temperature in this range include atmospheric convection, 3D hydrodynamical effects, and flux calibration (C. Genest-Beaulieu & P. Bergeron 2019).

On the other hand, there are other NOVs where the spectroscopic and photometric temperatures agree. For example, for J0127−2436 we find a spectroscopic temperature of $T_{\rm spec} = 11{,}557$ K compared to the photometric temperature $T_{\rm phot} = 11{,}236$ K. The spectroscopic method does not yield a significantly different temperature in this case, leaving this NOV still within the bounds of the photometric ZZ Ceti strip. It is interesting to note that the red edge of the spectroscopically determined instability strip is about 600 K hotter at $\approx 1.2 M_\odot$, potentially placing this star outside of the instability strip. The photometric and spectroscopic temperatures are in agreement, yet whether the star is within the instability strip or not is unclear. Again, the red edge of the photometric strip possibly needs to be adjusted to exclude this star, but more observations of NOVs outside of the strip are required. While the temperature discrepancy can explain some of the NOVs in the strip, it cannot account for all of them.
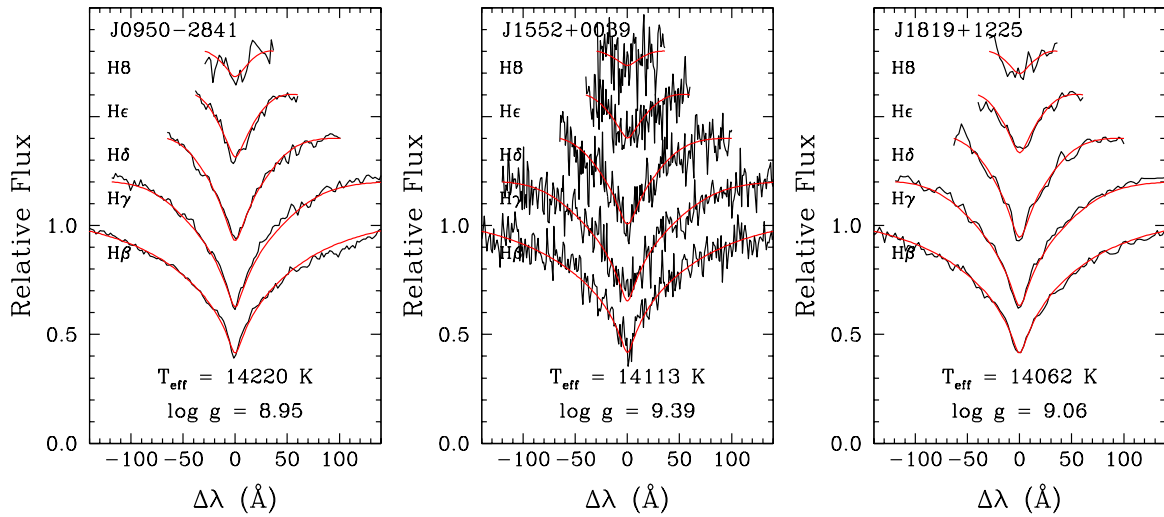
**Figure 15.** Spectroscopic model fits (red) to observed Balmer line profiles (black) of three NOV white dwarfs. The best-fitting effective temperature and log *g* are shown at the bottom of each panel. The effective temperatures and log *g* values have been corrected for 3D hydrodynamical effects (P. E. Tremblay et al. 2013).

Typically, massive white dwarfs are assumed to have CO cores and ultramassive white dwarfs are assumed to have ONe cores. However, the actual composition of the cores in ultramassive white dwarfs remains uncertain. Ultramassive white dwarfs are formed either through single stellar evolution with a single progenitor or through binary evolution with a merger event of two white dwarfs (K. D. Temmink et al. 2020). Both evolutionary channels can produce ultramassive white dwarfs with CO and ONe cores, leaving the true nature of ultramassive white dwarf interiors unresolved (see the discussion in M. E. Camisassa et al. 2021).

White dwarf mass estimates depend on the assumed core composition. For example, an ONe core would imply a mass lower by $0.05\,M_\odot$ compared to the CO-core case for the pulsator J0959−1828. The majority of the NOVs in our sample are located well within the instability strip boundaries where small mass differences would not make a significant difference in the white dwarf's location relative to the boundaries, see Figure 14. For the purposes of this study, assuming a CO-core composition is sufficient.

4. There is the possibility for some pulsation modes to show no (or very little) variation for some specific geometry, or its possible that destructive interference between two or more oscillation modes can also lower the pulsation amplitudes below the detection threshold (A. Gianninas et al. 2011). Given these caveats, perhaps it is not surprising that there are NOVs within the instability strip for massive white dwarfs.

### 5.5. Potential Rotational Multiplets

A well-known characteristic of nonradial stellar pulsations is that the eigenfrequencies of modes with spherical degree $\ell$ may split into $2\ell + 1$ components due to stellar rotation. These components are distinguished by their azimuthal order $m$. Under the assumption of slow and rigid rotation, the frequency splitting is given by

$$\delta\nu_{\ell,k,m} = m(1 - C_{\ell,k})\Omega_{\mathrm{R}}, \qquad (1)$$

where $\Omega_{\mathrm{R}}$ is the stellar rotation frequency expressed in cyclic units (e.g. $\mu$Hz or c day$^{-1}$), $C_{\ell,k}$ is the Ledoux constant, and $m = 0, \pm 1, \pm 2, \ldots, \pm \ell$ (W. Unno et al. 1989). The condition

for the validity of this first-order expression requires that $\Omega_{\mathrm{R}} \ll \delta\nu_{\ell,k}$.

In a few of the ultramassive WDs in our sample, we identify closely spaced frequency multiplets that could in principle be interpreted as signatures of rotation. However, for several stars (e.g., J1106+1802 and J0039−0357) the derived rotation frequencies are of the same order as the pulsation frequencies themselves (rotation periods of $\sim 0.2$ hr correspond to $\delta\nu_\ell \sim 120$–140 c day$^{-1}$). This violates the slow-rotation condition, and therefore the simple Ledoux splitting expression cannot be applied in a strictly valid way. The frequency spacings we report should thus be regarded as "candidate multiplets," not secure detections of rotational splitting.

An additional complication arises from the fact that frequency differences in the range we observe correspond to period differences of $\sim 20$–100 s. Such spacings are comparable to the expected asymptotic g-mode period spacings for ultramassive WDs. For ONe-core models in the mass range $1.10$–$1.29\,M_\odot$ and effective temperatures within the ZZ Ceti instability strip, theoretical calculations predict asymptotic $\ell = 1$ spacings of $\sim 21$–39 s (see Figure 6 of F. C. De Gerónimo et al. 2019). While some of the observed spacings fall near this range, others are significantly larger, making it difficult to disentangle whether the structures are due to rotational splitting, consecutive radial overtones, or a combination of both effects. Similar cautions have been emphasized by S. D. Kawaler (2015).

We summarize the observed frequency patterns in Table 6. For each star we report the potential doublets, triplets, or higher-order structures and the corresponding mean frequency spacings. While these values could be consistent with rotationally split multiplets, we stress that unambiguous rotation periods cannot be derived from the present data. Additional observations and detailed modeling will be required to distinguish between true multiplets and intrinsic g-mode period spacings. For the remaining ultramassive white dwarfs in our sample, we do not find compelling evidence for the presence of rotationally split multiplets. This implies that additional data are required to resolve potential multiplet structures.

**Table 6**
Summary of Potential Rotationally Split Multiplets in Ultramassive White Dwarfs Presented in This Work

| Star Name | Multiplet Type | $\langle \delta\nu \rangle$ (c day$^{-1}$)/$P_{\rm rot}$ (hr) |
|---|---|---|
| J0039−0357 | Triplet & Doublet | 69.77/0.17 |
| J0158−2503 | Quadruplet ($\ell = 2$) | 10.40/0.25 |
| J0204+8713 | Doublet ($\ell = 1$) | 8.38/1.43 |
| J1106+1802 | Triplet | 60.80/0.20 |
| J2208+2059 | Doublet ($\ell = 1$) | 17.85/0.67 |

## 6. Conclusions

Here we present the first time-series photometry of 22 massive white dwarfs from the MWDD 100 pc sample that fall within the ZZ Ceti instability strip. Our full sample contains 31 white dwarfs in which we classify 16 as pulsators and 15 as nonvariable.

Overall, we find four pulsating white dwarfs with $M > 1.2\,M_\odot$, three of which are new discoveries. Among the new discoveries, two of the most interesting white dwarfs are J0039−0357 and J0959−1828. J0039−0357 was observed on five nights with different pulsation modes emerging and vanishing, with only one mode consistently found over the five nights. J0959−1828, is now the most massive pulsating white dwarf known with mass $1.320 \pm 0.0004\,M_\odot$.

There is a clear correlation between the weighted mean period and temperature; hotter pulsators tend to have shorter periods (J. C. Clemens 1993). Confirmation of this trend comes from other studies in the literature, as well as our sample (A. Kanaan et al. 2002; A. S. Mukadam et al. 2006). We find three outliers in our sample: J0634+3848, J0912−2642, and J1626+2533. J1626+2533 does not show consistent pulsation modes and J0634−3848 has both long and short modes. J0912−2642 potentially has low-amplitude modes that were below our detection limits. Additional observations of these white dwarfs will help constrain their nature.

We find a correlation between the weighted mean period and stellar mass. Theory predicts a decreasing period with increasing stellar mass, which we confirm. This is due to higher mass white dwarfs having a higher surface gravity, leading to larger Brunt–Väisälä frequencies and shorter pulsation periods. Even though crystallization restricts $g$-mode propagation and should lead to lower pulsation frequencies, its effect is smaller than the increasing Brunt–Väisälä frequencies with mass. This is the first time a large sample of pulsating white dwarfs is found to show this relationship between weighted mean period and stellar mass.

Pulsation periods and power mostly follow expectations. A. S. Mukadam et al. (2006) found power to increase as temperature decreases, peaking in the middle of the instability strip, then decreasing again toward the red edge of the strip. Our sample supports this trend as the white dwarfs in our sample found in the middle of the strip have the highest power. Additionally, our sample shows a decrease in power toward the red edge of the strip. On the blue edge, J0912−2642 and J1626+2533 have the lowest power in our sample, which is to be expected, but these two stars are outliers in our sample and require more observation.

Half of the white dwarfs we observed showed no pulsation modes despite falling within the bounds of the instability strip. This invites the question, why do we not detect pulsations in these white dwarfs? The best explanations for these phenomena are magnetism, low-amplitude variability below the detection threshold, and discrepancies in temperature estimates through the photometric and spectroscopic methods. Because magnetism could be suppressing pulsations, it is possible that the nonvariables we find in the middle of the strip are weakly magnetic (P. E. Tremblay et al. 2015; N. P. Gentile Fusillo et al. 2017) with fields beyond the detection limit of low-resolution spectroscopy (M. Kilic et al. 2015; G. Jewett et al. 2024). Our observations of J0959−1828 using ULTRACAM and HIPERCAM show that there are low-amplitude modes that we simply cannot detect with our current setup at APO, meaning more observations are required for the NOVs in the middle of the strip.

Our study presents a more complete picture of the ZZ Ceti instability strip for massive and ultramassive white dwarfs in the MWDD 100 pc sample. As massive and ultramassive ZZ Ceti white dwarfs are rare, these observations provide valuable insight into the most massive pulsators and trends within this class of white dwarfs. We plan on obtaining extensive time-series photometry of the most massive systems in this sample at APO, NTT/ULTRACAM, and GTC/HiPERCAM for detailed asteroseismology.

## Appendix A
## Additional Pulsators

### A.1. J0154+4700

J0154+4700 has a mass of $M = 1.077 \pm 0.014\,M_\odot$ and $T_{\rm eff} = 11{,}838 \pm 235$ K. We observed this white dwarf once on UT 2024 November 6. Figure 16 shows its light curve and the corresponding Fourier transform. This white dwarf clearly shows two significant modes with frequencies 190.7 and 204.9 c day$^{-1}$. Both of these are well over the detection limit
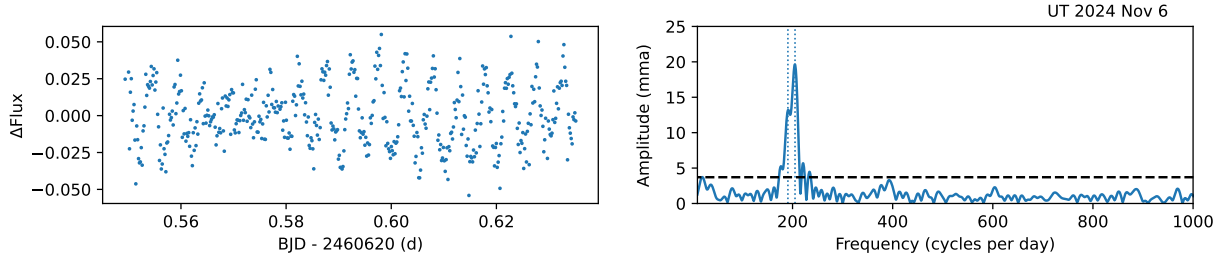
**Figure 16.** Light curve and Fourier transform for J0154+4700.

of 3.7 mma at amplitudes 13.8 and 20.2, respectively. Our goal in this study is to identify and confirm pulsating massive white dwarfs to study the sample properties, and we are able to confirm multiperiodic oscillations in this object based on this data. More extensive follow-up photometry on this target, as well as the other pulsators found in our survey would be required to characterize the pulsation spectrum of each object and to perform asteroseismology.

### A.2. J0204+8713

J0204+8713 has a mass of $M = 1.053 \pm 0.015 M_\odot$ and $T_{\rm eff} = 11{,}135 \pm 207$ K. This white dwarf was first identified as a pulsating white dwarf by O. Vincent et al. (2020), where they detected a single mode at 330 s. There were no spectra

available in the literature, but G. Jewett et al. (2024) confirmed this white dwarf to be a DA and presented the first night of data from UT 2023 April 15 further confirming the pulsations in this white dwarf. We obtained four additional nights of data on this target at APO, which are shown in Figure 17.

Again, with this white dwarf we detect different modes on different nights. On our first night of observation, UT 2023 April 15, we find two modes with frequencies 245.0 and 253.5 c day$^{-1}$. The second night, UT 2023 November 24, we detect three modes with frequencies 219.4, 228.0, and 260.3 c day$^{-1}$. On the third night, UT 2023 December 30, we only detect one mode at 266.6 c day$^{-1}$. Then on UT 2024 March 10, we detect the most modes. These have frequencies of 200.6, 231.9, 240.7, and 245.8 c day$^{-1}$. On the fifth night, on UT 2024 April 20, we find a single mode at 257.4 c day$^{-1}$.
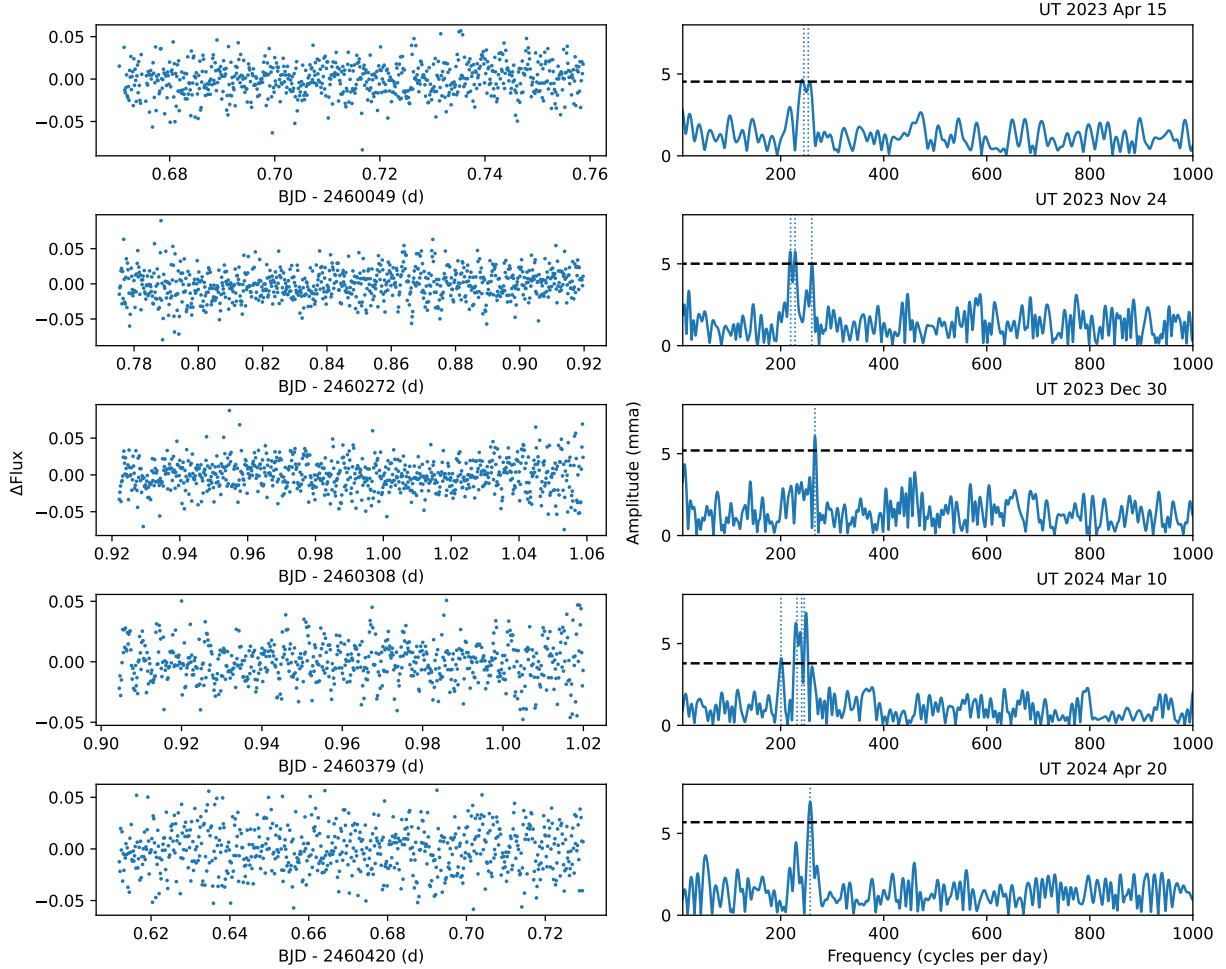


**Figure 17.** Light curves and Fourier transforms for J0204+8713 taken at APO.
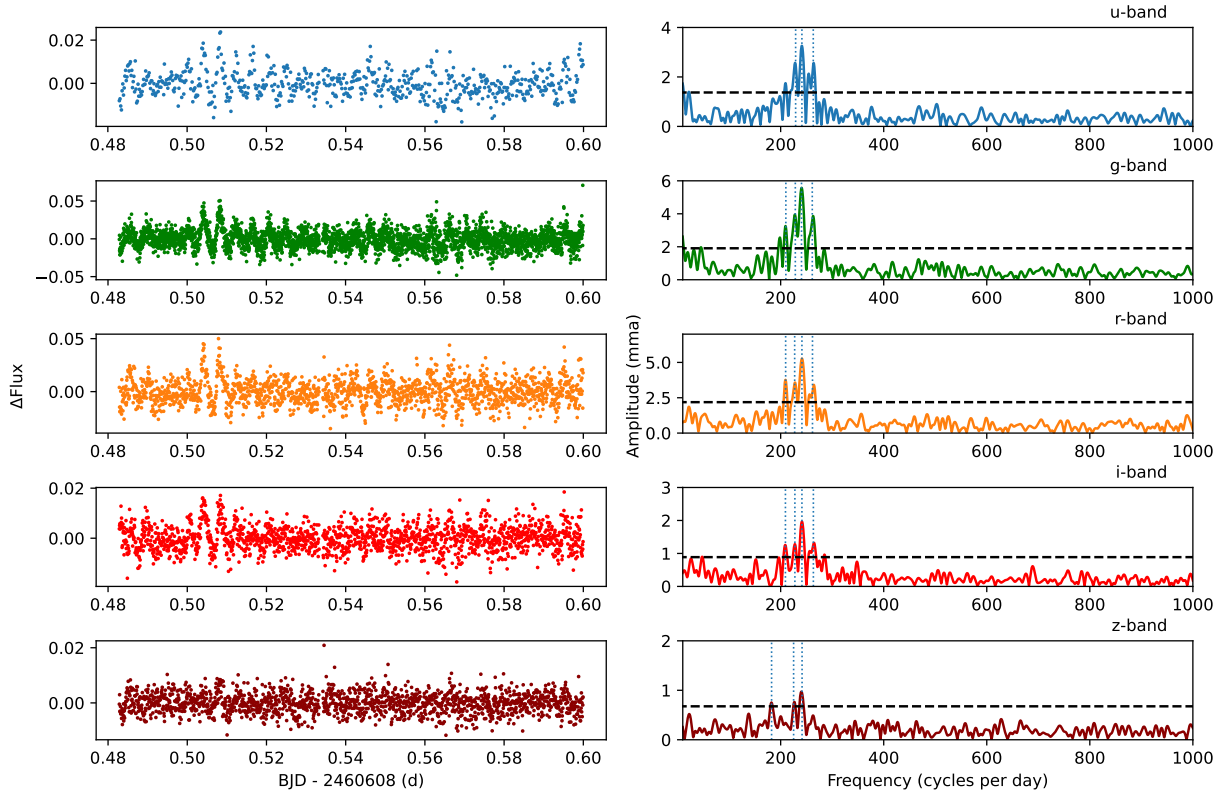
**Figure 18.** Light curves and Fourier transforms for J0204+8713 taken at GTC.

Finally on 2024 October 24, we observed J0204+8713 at GTC. Figure 18 shows the light curves and Fourier transforms for all five filters used. This observation run was 3.8 hr long, but due to telescope tracking issues we removed the last 1.0 hr of data. The g-band data has modes at 210.1, 228.4, 240.5, and 261.3 c day$^{-1}$. While we do not see the same modes on each night, the modes we see fall in a narrow frequency range of 200–266 cycles per day (or 324–430 s). The amplitudes for the modes we detect range from 3.4 to 9.1 mma.

### A.3. J0634+3848

This white dwarf was previously classified as NOV by O. Vincent et al. (2020) down to a limit of 2.3%. J0634+3848 has a mass of $M = 0.926 \pm 0.006\,M_\odot$ and $T_{eff} = 12{,}210 \pm 106$ K. We observed J0634+3848 on three different nights and detected pulsation modes on each night giving us confidence that this white dwarf is, in fact, pulsating. The light curves and corresponding Fourier transforms are shown in Figure 19.
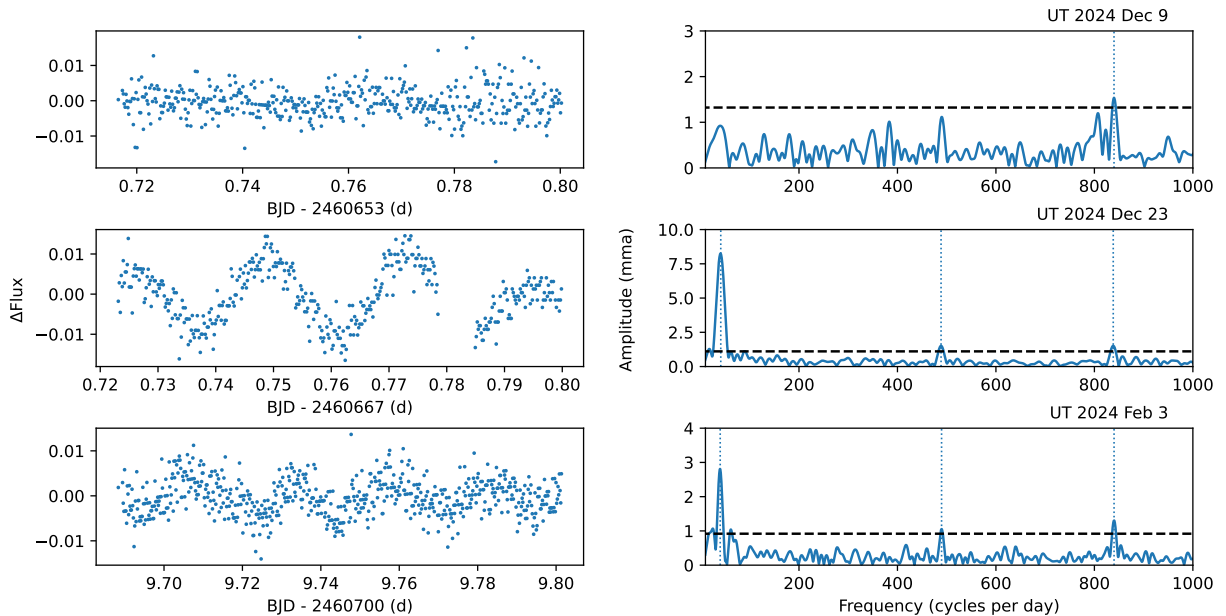


**Figure 19.** Light curves and Fourier transforms for J0634+3848.

On UT 2024 December 9, we find only one significant mode at 839.8 c day$^{-1}$. On the next night of observation, UT 2024 December 23, we detected three significant modes at 41.1, 488.6, and 838.3 c day$^{-1}$. During the last night of observations, UT 2025 February 3, we also detect three significant modes at 40.0, 489.6, and 839.9 c day$^{-1}$. The Fourier transform for J0634+3848 is clearly unusual. The mode at 103 s is clearly present in all three nights of data. The long period peak at $\sim$2100 s is unusual, as it is much longer than the pulsation periods seen in average mass or massive ZZ Ceti stars. Rapid rotation in spotted white dwarfs can cause such long-term trends, but we see the 2100 s mode only on two of the nights, and its amplitude is also significantly different on those two nights. Hence, J0634+3848 must be a pulsating white dwarf, but further follow-up observations are required to constrain its pulsation spectrum and understand its nature.

### A.4. J0712−1815

J0712−1815 has a mass of $0.980 \pm 0.008\ M_\odot$ and effective temperature $11{,}742 \pm 136$ K. J0712−1815 was observed on two different nights. We detect five modes each night of observations. On the first night, UT 2025 January 19, the modes are at 83.9, 151.7, 173.8, 205.5, and 256.9 c day$^{-1}$, whose amplitudes vary between 7−16 mma and are above the 4.3 mma significance level. We detect modes on UT 2025 February 5 at 85.4, 152.9, 170.7, 205.7, and 255.6 c day$^{-1}$, with amplitudes above the 3.2 mma significance level varying between 5 and 18 mma. The light curves and Fourier transforms are presented in Figure 20. The light curves from these two nights look fairly similar, and we detect roughly the same modes on each of these nights making this white dwarf one of our more consistent pulsators with multiple modes detected.
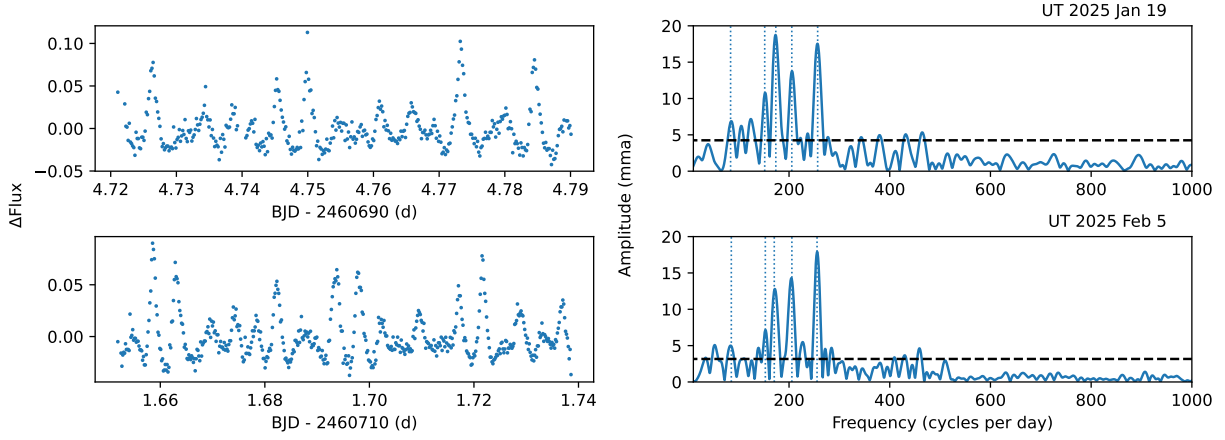


**Figure 20.** Light curves and Fourier transforms for J0712−1815.

### A.5. J1052+1610

J1052+1610 has mass $1.020 \pm 0.009$ $M_\odot$ and effective temperature $11{,}256 \pm 84$ K. We observed J1052+1610 on UT 2025 February 20 and detect two modes at 110.1 and 125.5 c day$^{-1}$ with amplitudes above the 2.7 mma significance level at 5 mma and 4.8 mma, respectively. The light curve and Fourier transform are shown in Figure 21.
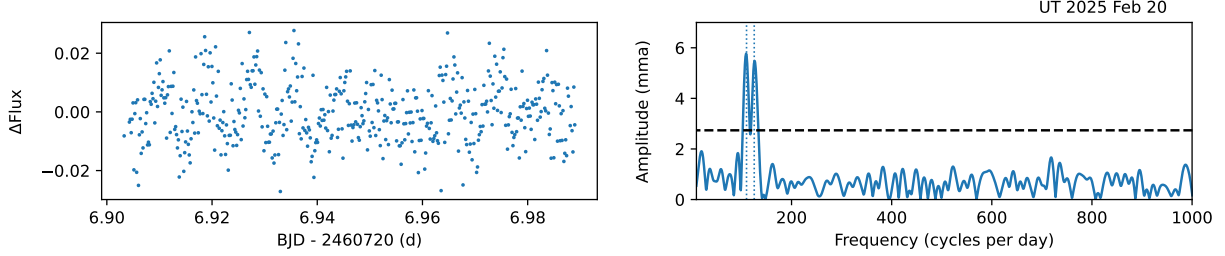


**Figure 21.** Light curve and Fourier transform for J1052+1610.

### A.6. J1451−2502

J1451−2502 has a mass of $1.016 \pm 0.011$ $M_\odot$ and effective temperature $11{,}189 \pm 97$ K. We were able to observe J1451−2502 on UT 2025 February 20 and we detected two modes at 152.4 and 181.9 c day$^{-1}$, both with amplitudes over the 6.1 mma significance level. The light curve and Fourier transform are shown in Figure 22.
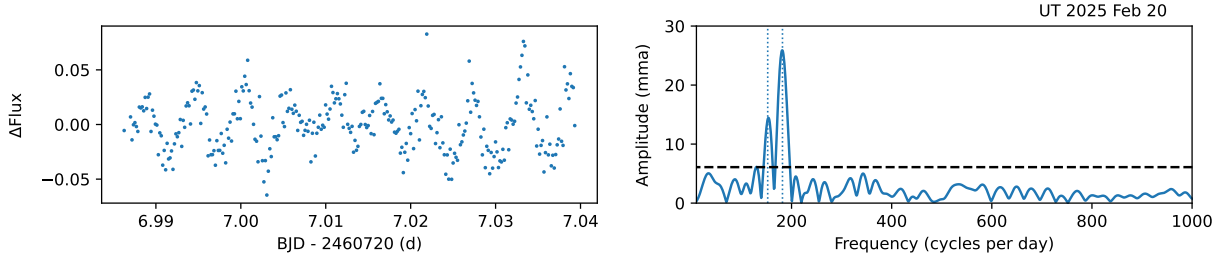


**Figure 22.** Light curve and Fourier transform for J1451−2502.

### A.7. J1722+3958

J1722+3958 has mass $0.997 \pm 0.010$ $M_\odot$ and effective temperature $11{,}069 \pm 109$ K. J1722+3959 was observed once on UT 2024 Aug 30. We find this white dwarf to have three modes at 180.6, 221.5, and 241.5 c day$^{-1}$, with amplitudes ranging from 8.1 to 19.7 mma. The light curve and Fourier transform are shown in Figure 23.
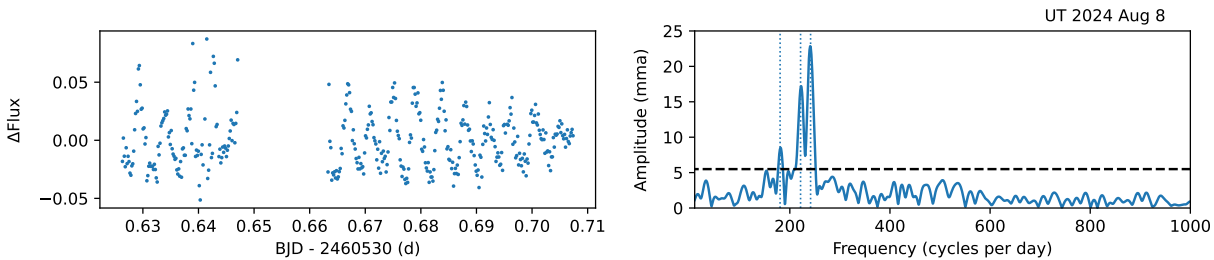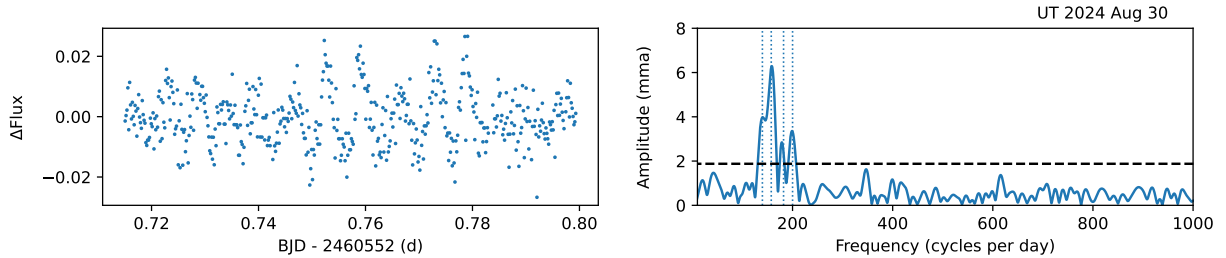


**Figure 23.** Light curve and Fourier transform for J1722+3958.

### A.8. J1929−2926

J1929−2926 has mass $1.054 \pm 0.016\ M_\odot$ and effective temperature $11{,}455 \pm 220$ K. J1929−2926 was observed once on UT 2024 August 8. We detected two modes at 201.7 and 231.1 c day$^{-1}$ with amplitudes 10.0 and 7.2, respectively. The light curve and Fourier transform are presented in Figure 24.
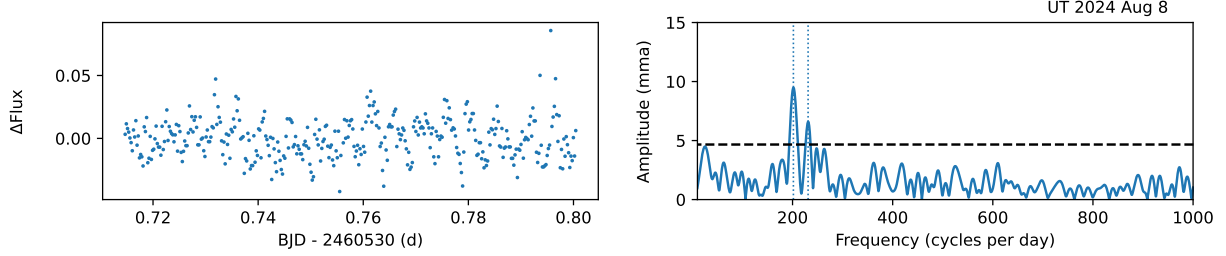


**Figure 24.** Light curve and Fourier transform for J1929−2926.

### A.9. J2026−2254

J2026−2254 has mass $0.917 \pm 0.008\ M_\odot$ and effective temperature $11{,}405 \pm 88$ K. On UT 2024 June 14, we detect two modes at 174.0 and 272.1 c day$^{-1}$ with amplitudes 35.8 mma and 11.5 mma. The light curve and Fourier transform are shown in Figure 25.
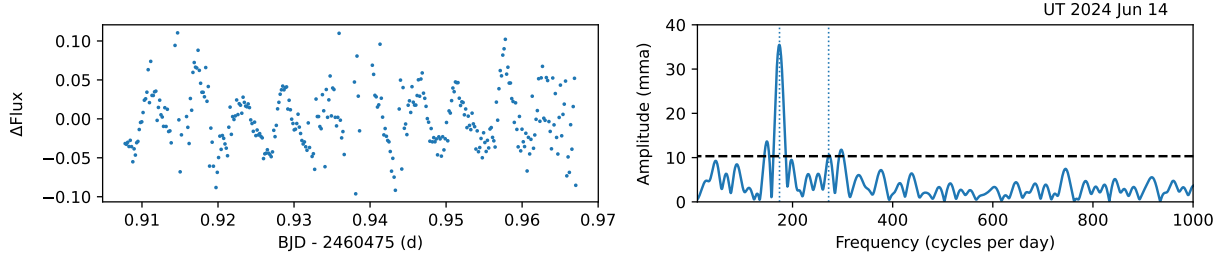


**Figure 25.** Light curve and Fourier transform for J2026−2254.

### A.10. J2208+2059

J2208+2059 has mass $0.941 \pm 0.011\ M_\odot$ and effective temperature $11{,}091 \pm 99$ K. We were able to observe this white dwarf once on UT 2024 Aug 30. We found four modes at 139.8, 157.5, 182.1, and 200.1 c day$^{-1}$ with amplitudes ranging from 2.2 to 7.4 mma. The light curve and Fourier transform are shown in Figure 26.



**Figure 26.** Light curve and Fourier transform for J2208+2059.

## Appendix B
## Not-observed-to-vary (NOV) White Dwarfs

Here we present the light curves and the corresponding Fourier transforms for 15 white dwarfs that do not show any significant variability in our follow-up data shown in Figure 27. Each row is labeled with the object name and the observation date. The last four objects (J1656+5719, J1819+1225, J1928+1526, and J2107+7831) were observed on two different nights, and both nights of data do not show any significant pulsation modes. The 4 $\langle A \rangle$ detection limits range from 1.5 mma in the best case (J0725 +0411) to 7.7 mma in the worst case (J1928+1526), with a median at 3.1 mma. These detection limits are included in Table 7. In addition, we observed J0408+2323 and J0657+7241

at GTC using HiPERCAM shown in Figures 28 and 29. We show all five filters of data, with each filter labeled above the corresponding Fourier transform. The detection limits (4$\langle A \rangle$) are listed in Table 8. There was also no significant variability detected in these observations that would indicate these stars are pulsating. There are two low frequency peaks in the g-band data in the GTC data for J0657+7241. These peaks have periods of 3223.0 and 5162.8 s. These periods are too long to be from pulsations and are more likely from rotation. Furthermore, if this white dwarf was weakly magnetic, this could explain why it is not pulsating. We tentatively classify this star as variable due to rotation, but further observations are required to constrain these peaks.

**Table 7**
Observation Details and Detection Limits for Targets That Are Not Observed to Vary (NOV) Taken at APO

| Object Name | UT Date | Length (hr) | 4$\langle A \rangle$ (mma) |
| --- | --- | --- | --- |
| J0050−2826 | 2024 Dec 9 | 1.9 | 5.3 |
| J0127−2436 | 2024 Dec 21 | 1.4 | 7.2 |
| J0408+2323 | 2024 Nov 21 | 2.0 | 2.3 |
| J0538+3212 | 2024 Dec 1 | 2.1 | 1.8 |
| J0657+7341 | 2024 Nov 21 | 2.0 | 3.4 |
| J0725+0411 | 2024 Dec 25 | 2.6 | 1.5 |
| J0949−0730 | 2025 Feb 9 | 1.7 | 3.2 |
| J0950−2841 | 2025 Mar 9 | 2.2 | 6.2 |
| J1243+4805 | 2024 May 18 | 2.0 | 2.1 |
| J1342−1413 | 2024 Apr 20 | 1.5 | 2.0 |
| J1552+0039 | 2024 Jun 6 | 2.0 | 3.3 |
| J1656+5719 | 2024 Aug 11 | 2.6 | 1.9 |
| J1656+5719 | 2024 Sep 1 | 2.2 | 2.2 |
| J1819+1225 | 2024 Jun 14 | 1.9 | 3.1 |
| J1819+1225 | 2024 Sep 13 | 1.5 | 5.4 |
| J1928+1526 | 2024 Aug 29 | 1.3 | 2.8 |
| J1928+1526 | 2024 Sep 15 | 1.7 | 7.7 |
| J2107+7831 | 2024 Aug 29 | 2.0 | 2.4 |
| J2107+7831 | 2024 Sep 13 | 1.1 | 4.4 |

**Table 8**
Observation Details and Detection Limits for Targets That Are Not Observed to Vary (NOV) Taken at GTC

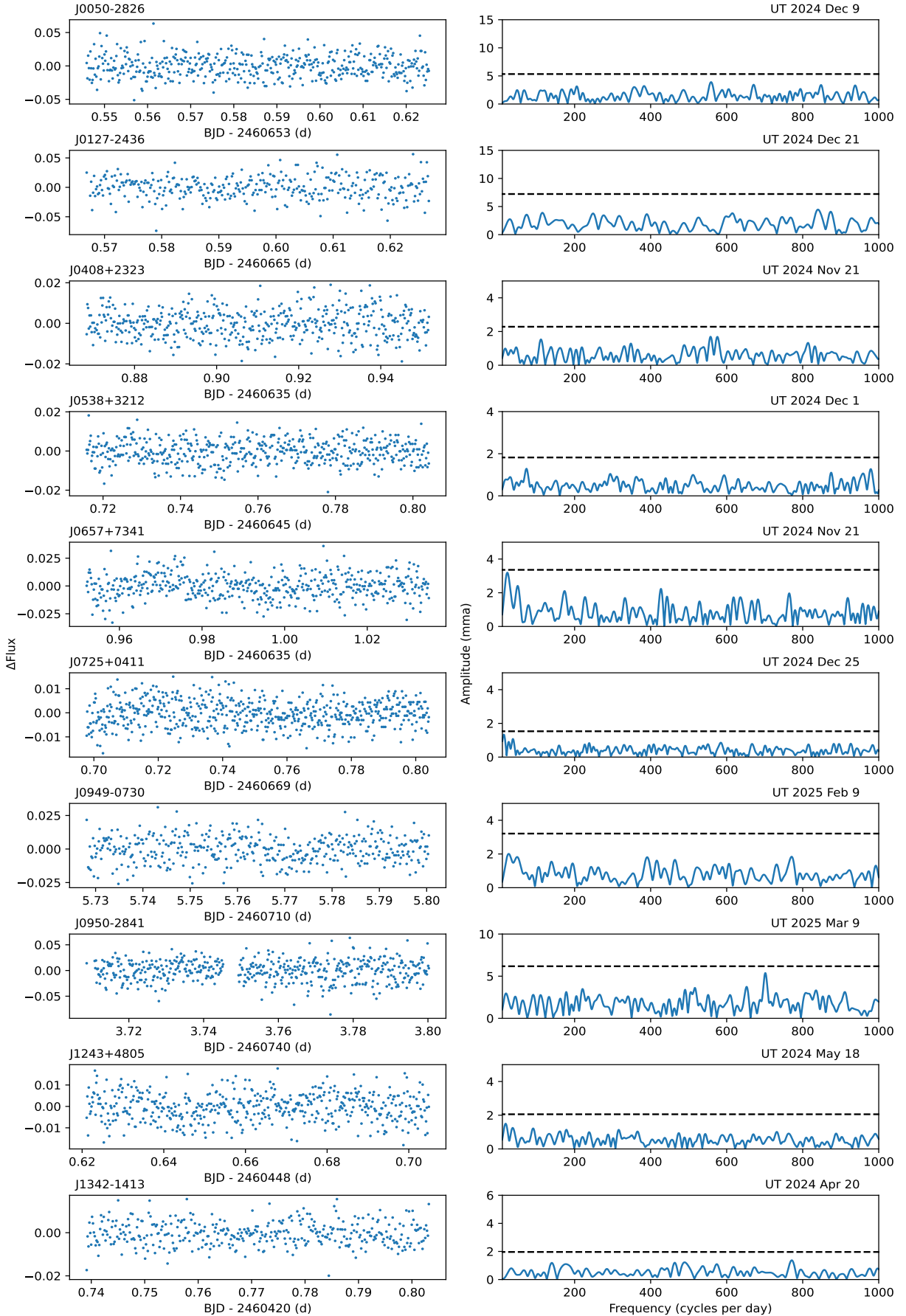| Object Name | UT Date | Length (hr) | 4$\langle A \rangle$ (mma) |
| --- | --- | --- | --- |
| J0408+2323 *u*-band | 2025 Jan 16 | 2.7 | 0.4 |
| J0408+2323 *g*-band | | | 0.5 |
| J0408+2323 *r*-band | | | 0.2 |
| J0408+2323 *i*-band | | | 0.2 |
| J0408+2323 *z*-band | | | 0.2 |
| J0657+7341 *u*-band | 2025 Jan 10 | 4.0 | 3.2 |
| J0657+7341 *g*-band | | | 0.5 |
| J0657+7341 *r*-band | | | 0.5 |
| J0657+7341 *i*-band | | | 0.4 |
| J0657+7341 *z*-band | | | 0.4 |

**Figure 27.** The left panels show the light curves for nonvariable white dwarfs in our sample. The right panels show the corresponding Fourier transforms with the observation date labeled on top. The dashed black lines mark the $4\langle A \rangle$ detection limits, which are listed in Table 7.
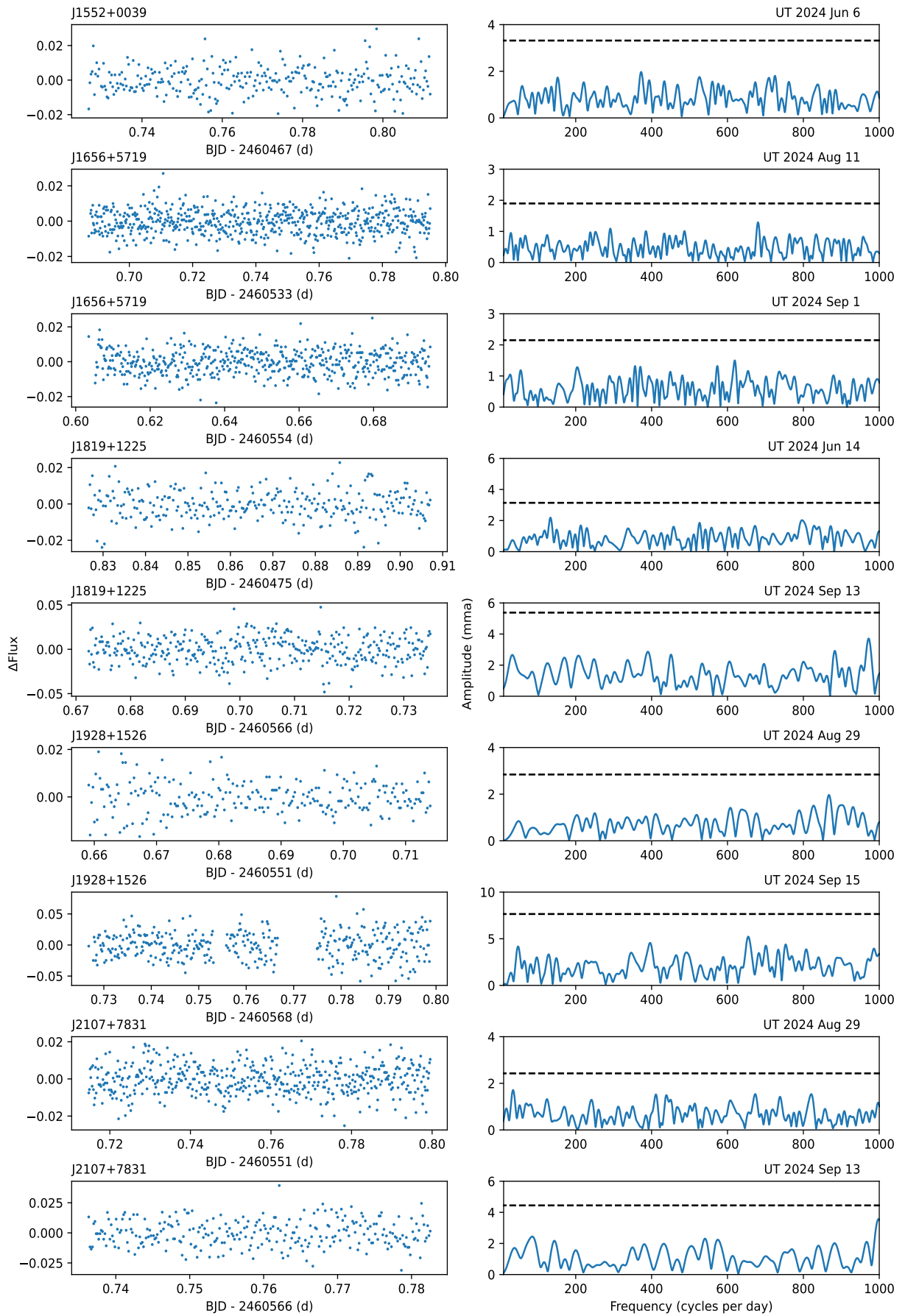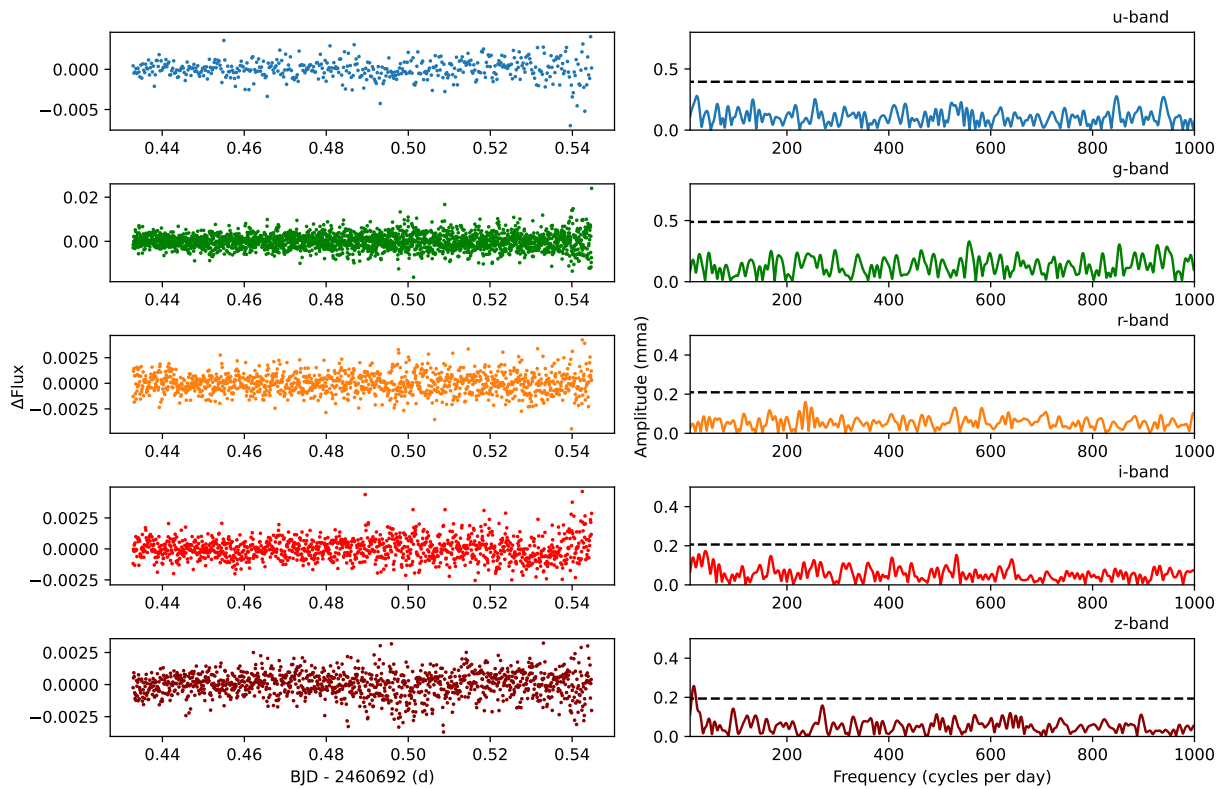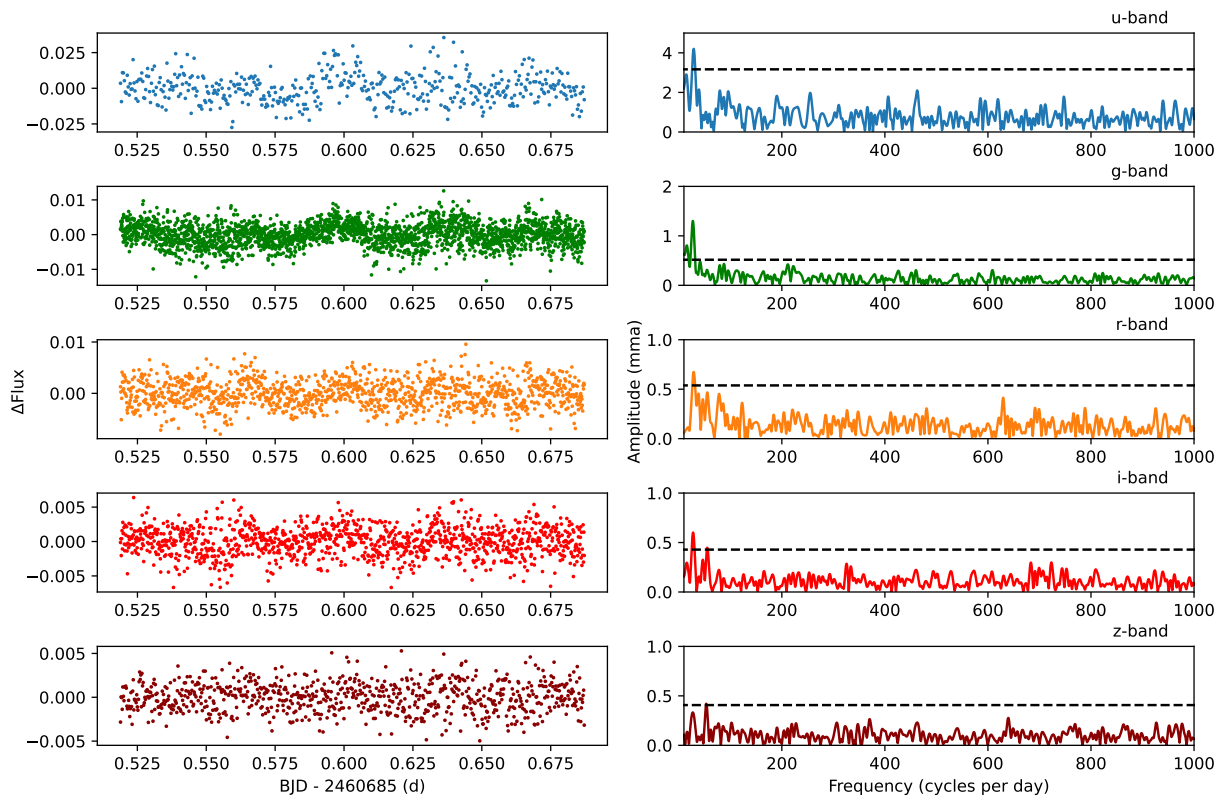
**Figure 27.** (Continued.)

**Figure 28.** Light curves and Fourier transforms for J0408+2323.



**Figure 29.** Light curves and Fourier transforms for J0657+7341.

## ORCID iDs

Gracyn Jewett ● https://orcid.org/0009-0009-9105-7865
Mukremin Kilic ● https://orcid.org/0000-0001-6098-2235
Adam Moss ● https://orcid.org/0000-0001-7143-0890
Alejandro H. Córsico ● https://orcid.org/0000-0002-0006-9900
Matthew J. Green ● https://orcid.org/0000-0002-0948-4801
Murat Uzundag ● https://orcid.org/0000-0002-6603-994X
Pierre Bergeron ● https://orcid.org/0000-0003-2368-345X
Warren R. Brown ● https://orcid.org/0000-0002-4462-2341
Francisco C. De Gerónimo ● https://orcid.org/0000-0002-8079-0772
Alberto Rebassa-Mansergas ● https://orcid.org/0000-0002-6153-7173
Alex J. Brown ● https://orcid.org/0000-0002-3316-7240
Vikram S. Dhillon ● https://orcid.org/0000-0003-4236-9642
Stuart Littlefair ● https://orcid.org/0000-0001-7221-855X

## References

Althaus, L. G., Córsico, A. H., Isern, J., & García-Berro, E. 2010, A&ARv, 18, 471
Bagnulo, S., & Landstreet, J. D. 2022, ApJL, 935, L12
Bergeron, P., Dufour, P., Fontaine, G., et al. 2019, ApJ, 876, 67
Bergeron, P., Fontaine, G., Billères, M., Boudreault, S., & Green, E. M. 2004, ApJ, 600, 404
Bradley, P. A. 1996, ApJ, 468, 350
Breger, M., Stich, J., Garrido, R., et al. 1993, A&A, 271, 482
Brown, A. J., Parsons, S. G., Littlefair, S. P., et al. 2022, MNRAS, 513, 3050
Caliskan, O., Uzundag, M., Kilic, M., et al. 2025, ApJ, 988, 32
Camisassa, M. E., Althaus, L. G., Torres, S., et al. 2021, A&A, 649, L7
Castanheira, B. G., Kepler, S. O., Costa, A. F. M., et al. 2007, A&A, 462, 989
Castanheira, B. G., Kepler, S. O., Kleinman, S. J., Nitta, A., & Fraga, L. 2010, MNRAS, 405, 2561
Clemens, J. C. 1993, BaltA, 2, 407
Córsico, A. H., Althaus, L. G., Miller Bertolami, M. M., & Kepler, S. O. 2019, A&ARv, 27, 7
Curd, B., Gianninas, A., Bell, K. J., et al. 2017, MNRAS, 468, 239
De Gerónimo, F. C., Córsico, A. H., Althaus, L. G., Wachlin, F. C., & Camisassa, M. E. 2019, A&A, 621, A100
De Gerónimo, F. C., Uzundag, M., Rebassa-Mansergas, A., et al. 2025, ApJL, 980, L9
Dhillon, V. S., Bezawada, N., Black, M., et al. 2021, MNRAS, 507, 350
Dhillon, V. S., Marsh, T. R., Stevenson, M. J., et al. 2007, MNRAS, 378, 825

Dufour, P., Blouin, S., Coutu, S., et al. 2017, in ASP Conf. Ser. 509, 20th European White Dwarf Workshop, ed. P. E. Tremblay, B. Gaensicke, & T. Marsh (San Francisco, CA: ASP), 3
Fontaine, G., Brassard, P., & Bergeron, P. 2001, PASP, 113, 409
Genest-Beaulieu, C., & Bergeron, P. 2019, ApJ, 871, 169
Gentile Fusillo, N. P., Tremblay, P.-E., Jordan, S., et al. 2017, MNRAS, 473, 3693
Gianninas, A., Bergeron, P., & Fontaine, G. 2005, ApJ, 631, 1100
Gianninas, A., Bergeron, P., & Ruiz, M. T. 2011, ApJ, 743, 138
Guidry, J. A., Vanderbosch, Z. P., Hermes, J. J., et al. 2021, ApJ, 912, 125
Hermes, J. J., Kepler, S. O., Castanheira, B. G., et al. 2013, ApJL, 771, L2
Hermes, J. J., Montgomery, M. H., Winget, D. E., et al. 2013, ApJ, 765, 102
Jewett, G., Kilic, M., Bergeron, P., et al. 2024, ApJ, 974, 12
Kanaan, A., Kepler, S. O., Giovannini, O., & Diaz, M. 1992, ApJL, 390, L89
Kanaan, A., Kepler, S. O., & Winget, D. E. 2002, A&A, 389, 896
Kawaler, S. D. 2015, in ASP Conf. Ser. 493, 19th European Workshop on White Dwarfs, ed. P. Dufour, P. Bergeron, & G. Fontaine (San Francisco, CA: ASP), 65
Kilic, M., Bergeron, P., Blouin, S., et al. 2025, ApJ, 979, 157
Kilic, M., Bergeron, P., Kosakowski, A., et al. 2020, ApJ, 898, 84
Kilic, M., Córsico, A. H., Moss, A. G., et al. 2023a, MNRAS, 522, 2181
Kilic, M., Gianninas, A., Bell, K. J., et al. 2015, ApJL, 814, L31
Kilic, M., Hermes, J. J., Córsico, A. H., et al. 2018, MNRAS, 479, 1267
Kilic, M., Moss, A. G., Kosakowski, A., et al. 2023b, MNRAS, 518, 2341
Landolt, A. U. 1968, ApJ, 153, 151
Lenz, P. 2005, CoAst, 146, 53
Metcalfe, T. S., Montgomery, M. H., & Kanaan, A. 2004, ApJ, 605, L133
Montgomery, M. H. 2005, ApJ, 633, 1142
Montgomery, M. H., & Winget, D. E. 1999, ApJ, 526, 976
Mukadam, A. S., Montgomery, M. H., Winget, D. E., Kepler, S. O., & Clemens, J. C. 2006, ApJ, 640, 956
Mukadam, A. S., Winget, D. E., von Hippel, T., et al. 2004, ApJ, 612, 1052
O'Brien, M. W., Tremblay, P. E., Klein, B. L., et al. 2024, MNRAS, 527, 8687
Romero, A. D., Kepler, S. O., Hermes, J. J., et al. 2022, MNRAS, 511, 1574
Rui, N. Z., Fuller, J., & Hermes, J. J. 2025, ApJ, 981, 72
Tassoul, M., Fontaine, G., & Winget, D. E. 1990, ApJS, 72, 335
Temmink, K. D., Toonen, S., Zapartas, E., Justham, S., & Gänsicke, B. T. 2020, A&A, 636, A31
Tremblay, P. E., Fontaine, G., Freytag, B., et al. 2015, ApJ, 812, 19
Tremblay, P. E., Ludwig, H. G., Steffen, M., & Freytag, B. 2013, A&A, 559, A104
Unno, W., Osaki, Y., Ando, H., Saio, H., & Shibahashi, H. 1989, Nonradial Oscillations of Stars (Tokyo: Univ. Tokyo Press)
Uzundag, M., Kilic, M., De Gerónimo, F.C., et al. 2025, ApJ, Submitted
Van Grootel, V., Dupret, M. A., Fontaine, G., et al. 2012, A&A, 539, A87
Vincent, O., Barstow, M. A., Jordan, S., et al. 2024, A&A, 682, A5
Vincent, O., Bergeron, P., & Lafrenière, D. 2020, AJ, 160, 252